JOURNAL OF THERMOPHYSICS AND HEAT TRANSFER
Vol. 21, No. 2, April–June 2007

Electromagnetic Fluid Dynamics for Aerospace Applications

Domenic D'Ambrosio*
Politecnico di Torino, 10129 Torino, Italy
and
Domenico Giordano†
ESA, 2200 AG Noordwijk, The Netherlands

DOI: 10.2514/1.24732

Starting from the basic and general approach founded on the coupling between the Maxwell and the Navier–Stokes equations, the authors review some physical and mathematical models that are currently used in the aerospace engineering community for representing the behavior of electrically conducting flows subject to electromagnetic fields. Then, they present four different numerical methods for solving the magnetofluid dynamics equations in different formulations and for different magnetic Reynolds number regimes. For the sake of simplicity, the attention is focused on one-dimensional cases. Finally, numerical results obtained using the above mentioned numerical techniques on a magnetofluid dynamics shock-tube problem are compared and discussed.

Nomenclature

$\boldsymbol{B}$	=	magnetic field density
c	=	speed of light in vacuum, $\sim 2.998 \times 10^8$ m/s
$\boldsymbol{E}$	=	electric field
E_t	=	total energy
e_m	=	matter energy
$\boldsymbol{F}$	=	flux vector
$\boldsymbol{I}$	=	identity matrix
$\boldsymbol{J}_Q$	=	conduction-current density
$\boldsymbol{J}_U$	=	internal energy diffusive flux
$\boldsymbol{j}$	=	electric current density
K	=	loading parameter
M	=	Mach number
$\boldsymbol{n}$	=	normal unit vector
p	=	pressure
Q	=	magnetic interaction parameter
Re	=	Reynolds number
Re_m	=	magnetic Reynolds number
S	=	magnetic force number
$\mathcal{S}$	=	finite control surface
T	=	temperature
t	=	time
V	=	velocity magnitude
$\mathcal{V}$	=	finite control volume
$\boldsymbol{v}$	=	velocity vector
$\boldsymbol{W}$	=	conservative variables vector
γ	=	specific heats ratio
ε_0	=	permittivity of vacuum, $\sim 8.854 \times 10^{-12}$ F/m
λ_e	=	scalar electrical conductivity
$\boldsymbol{\lambda}_e$	=	electrical conductivity tensor
μ	=	dynamic viscosity
ρ	=	density
ρ_c	=	electric charge density
$\boldsymbol{\tau}$	=	stress tensor
ϕ	=	electric potential
$\boldsymbol{\Omega}$	=	source terms vector

Subscripts

app	=	applied
i	=	variable number
ind	=	induced
x, y, z	=	vector components in the coordinate directions
∞	=	freestream conditions
0	=	characteristic value

Presented as Paper 2362 at the AIAA Plasmadynamics and Lasers Conference, Portland, OR, 28 June–7 January 2004; received 20 April 2006; revision received 27 July 2006; accepted for publication 28 July 2006.

*Assistant Professor, Dipartimento di Ingegneria Aeronautica e Spaziale, Corso Duca degli Abruzzi 24; domenic.dambrosio@polito.it.

†Research Engineer, European Space Research and Technology Center, Aerothermodynamics Section, Keplerlaan 1; Domenico.Giordano@esa.int.

I. Introduction

IN the quest for new physical mechanisms for flowfield control, the appealing possibility of manipulating a natural or artificially enhanced electrically conductive flowfield with a suitably imposed magnetic field has recently renewed the interest of the aerospace community in the multidisciplinary subject of magnetofluid dynamics (MFD) [1–3].

Presently, several efforts are carried out in different countries with the aim of providing a better understanding of the basic underlying physical mechanisms and to investigate whether or not magnetofluid dynamic flow control is efficiently feasible. Beside experimental campaigns, which are of inestimable value, but that cannot be very numerous because of cost and technical difficulty, a large number of numerical simulations are performed. In this framework, computational magnetofluid dynamics (CMFD) represents one of the most promising interdisciplinary computational technologies for aerospace-vehicle design [4].

Computations are based on mathematical models that describe a physical representation of the real world. The choice of a model and thus the acceptance of all the underlying hypotheses, determines the nature of the results that numerical computations provide.

The physical phenomenology and the theoretical background within which we operate are described in [3]; the set of governing equations discussed therein will be referred to as the *full magnetofluid dynamics (FMFD) equations*. The latter are composed of the Maxwell equations coupled with the mass, momentum, and energy balance equations for a conducting fluid in the presence of an electromagnetic field. Starting from this basic and general approach, a variety of reduced models, based on different assumptions and addressed to different scientific and technological fields, have been developed and are available in the literature [1,5]. The different sets of governing equations will be referred to as the *simplified magnetofluid dynamics equations (SMFD)*. In the SMFD model, the Maxwell equations are replaced by the magnetic induction equation. In addition, borderline situations may arise when some of the nondimensional parameters that appear in the SMFD equations are

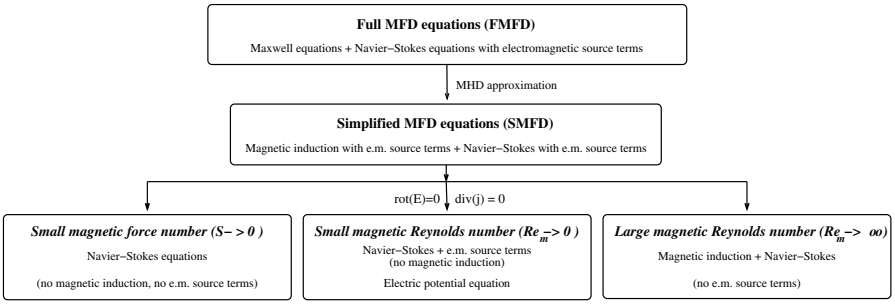

Fig. 1 Schematic view of the MFD physical models.

very large or very small. The above depicted classification is schematized in Fig. 1. In principle, thermochemical nonequilibrium models should be also coupled to the governing MFD equations to account for variable chemical composition and transport coefficients that depend on the nature of the ionized gas. Here, such a physically important aspect will be omitted to simplify the discussion on numerical methodologies for MFD, which are not modified by the presence of high-temperature models.

In the following, after a review of the physical and mathematical models that are now used in the simulation of magnetofluid dynamic problems in the framework of aerospace applications, numerical methods for solving both the full and the simplified magnetofluid dynamics equations for one-dimensional flows are proposed. These methods are the building blocks for constructing numerical codes for multidimensional problems.

II. Full Magnetofluid Dynamics Equations

A. Full Magnetofluid Dynamics Equations In Nondimensional Form

At this stage, we write the full magnetofluid dynamics equations in nondimensional form. In the following, the reference value for any variable will be indicated with the subscript 0, except for the characteristic length, which will be defined as L. For the sake of simplicity, we will restrict the expression of the conduction-current density to Ohm law:

$$\boldsymbol{J}_Q = \boldsymbol{\lambda}_e(\boldsymbol{E} + \boldsymbol{v} \times \boldsymbol{B}) \tag{1}$$

The pressoelectrical- and thermoelectrical-conductivity contributions to $\boldsymbol{J}_Q$ [Eq. (131) of [3]] have been neglected. From a mathematical point of view, however, the assumed form of the conduction-current density does not change the nature of the equation set. The anisotropic nature of the plasma is embedded in the tensorial form of $\boldsymbol{\lambda}_e$, which accounts for the *Hall* and for the *ion slip* effects [6].

As standard [5], we take $V_0 = \sqrt{R_0 T_0}$, B_0, ρ_0, T_0, μ_0, λ_{e0}, and L as fundamental reference values to make nondimensional the governing equations. The reference pressure is given by

$$p_0 = \rho_0 V_0^2 \tag{2}$$

Frequently, the so-called *loading parameter* K is introduced as ratio between the reference electric field E_0 and product $V_0 B_0$, so that

$$K = \frac{E_0}{V_0 B_0} \tag{3}$$

Finally, the reference electric-charge density ρ_{c0} is defined using Gauss' law for electricity:

$$\rho_{c0} = \varepsilon_0 \frac{E_0}{L} = \varepsilon_0 K \frac{V_0 B_0}{L} \tag{4}$$

Using the reference values defined above, it is possible to define a set of similarity parameters for MFD. In particular, we have

$$M = \frac{V_\infty}{\sqrt{\gamma p_0/\rho_0}} = \frac{V_\infty}{\sqrt{\gamma} V_0} \qquad \text{Mach number} \tag{5}$$

$$Re = \frac{\rho_0 V_\infty L}{\mu_0} = \frac{\rho_0 V_0 L}{\mu_0}\sqrt{\gamma} M \qquad \text{Reynolds number} \tag{6}$$

$$Re_m = \frac{\lambda_{e0} V_\infty L}{\epsilon_0 c^2} = \frac{\lambda_{e0} V_0 L}{\epsilon_0 c^2}\sqrt{\gamma} M \qquad \text{magnetic Reynolds number} \tag{7}$$

$$Q = S Re_m = \frac{\lambda_{e0} B_0^2 L}{\rho_0 V_0} \qquad \text{magnetic interaction parameter} \tag{8}$$

$$S = \frac{\epsilon_0 c^2 B_0^2}{\rho_0 V_\infty^2} = \frac{\epsilon_0 c^2 B_0^2}{\rho_0 V_0^2}\frac{1}{\gamma M^2} \qquad \text{magnetic force number} \tag{9}$$

The full magnetofluid dynamics equations can be written in nondimensional form in such a way that the similarity parameters defined above are put in evidence.

$$\frac{\partial \rho}{\partial t} + \nabla \cdot (\rho \boldsymbol{v}) = 0 \tag{10a}$$

$$\frac{\partial \rho \boldsymbol{v}}{\partial t} + \nabla \cdot (\rho \boldsymbol{v}\boldsymbol{v} + p\boldsymbol{I}) - \frac{\sqrt{\gamma} M}{Re}\nabla \cdot \boldsymbol{\tau} = K \frac{V_\infty^2}{c^2} S \rho_c (K\boldsymbol{E} + \boldsymbol{v} \times \boldsymbol{B}) + \sqrt{\gamma} M Q \boldsymbol{J}_Q \times \boldsymbol{B} \tag{10b}$$

$$\frac{\partial (\rho e_m)}{\partial t} + \nabla \cdot [(\rho e_m + p)\boldsymbol{v}] + \frac{\sqrt{\gamma} M}{Re}\nabla \cdot (\boldsymbol{J}_U - \boldsymbol{\tau} \cdot \boldsymbol{v}) = K^2 \frac{V_\infty^2}{c^2} S \rho_c \boldsymbol{v} \cdot \boldsymbol{E} + K\sqrt{\gamma} M Q \boldsymbol{J}_Q \cdot \boldsymbol{E} \tag{10c}$$

$$K(\nabla \times \boldsymbol{E}) = -\frac{\partial \boldsymbol{B}}{\partial t} \tag{10d}$$

$$\nabla \times \boldsymbol{B} = \frac{K}{\gamma M^2}\frac{V_\infty^2}{c^2}\left(\rho_c \boldsymbol{v} + \frac{\partial \boldsymbol{E}}{\partial t}\right) + \frac{Re_m}{\sqrt{\gamma} M}\boldsymbol{J}_Q \tag{10e}$$

All magnetofluid dynamics variables are now to be intended as nondimensional. Of course, the consideration of chemical kinetics is fundamental for the present problem and consequently the components mass balance equations [Eq. (19) of [3]], whose solution is necessary for the evaluation of the mixture chemical composition and transport properties, should also be included in the set of Eqs. (10). Here, they have not been explicitly included only because their presence does not change the nature of the coupling

between electromagnetism and fluid dynamics, which is the focal point of the paper. Indeed, when numerical methods will be discussed in Secs. IV and V, a scalar and uniform electrical conductivity will be used for simplicity, but the basics of the adopted numerical methodology would not be different in case $\boldsymbol{\lambda}_e$ were obtained from a high-temperature flow computation.

The adoption of the FMFD model is interesting for different reasons. One is to prove the validity of the simplifying assumptions of MFD through extensive comparison of numerical results obtained using both full and simplified models in a wide range of conditions. Another one is related to the independence of the full MFD model from the generalized Ohm law, which makes it possible to use different approximations for the conduction current in case it were necessary. A third reason is that a numerical method for the FMFD equations can be used without encountering numerical difficulties starting from conditions of zero electrical conductivity up to medium/high values of the latter. Conversely, the usual numerical treatment of the full SMFD models is numerically robust only when the magnetic Reynolds number is not too small (i.e., medium/high). In Sec. V.B, however, a numerical technique to solve the SMFD equations will be described that works well for small to medium values of Re_m. Finally, the low-Re_m SMFD model can be applied by definition only when the magnetic Reynolds number is very small everywhere in the flowfield, that is when the presence of an induced magnetic field is negligible.

III. Simplified Magnetofluid Dynamics Equations

The nondimensional form of the full MFD equations defined in Eqs. (10) provides information that can be used to neglect some of its terms. In aerospace applications, the typical order of magnitude of the similarity parameters is $Re_m \simeq 1 \div 10$, $S \simeq 0.1 \div 100$, and $Q \simeq 0.1 \div 1000$. Because $V_\infty \simeq 10 \div 1000$ m/s, it is $V_\infty^2/c^2 \simeq 10^{-15} \div 10^{-11}$. Thus, it seems reasonable to assume that all terms that are multiplied by V_∞^2/c^2 in Eqs. (10a–10e), that is all terms containing the electric-charge density and the displacement-current density can be considered small with respect to the others and therefore neglected. Also in case of a high frequency electric field, Sutton and Sherman [5] note that even at microwave frequency the displacement current could be neglected. The above observations are usually reasonable in some engineering applications, but one cannot exclude a priori situations where their validity may break up as, for instance, inside a hypersonic boundary layer. After all, before the historic paper [7] given by Ludwig Prandtl in 1904,[‡] fluid dynamicists found themselves in the paradoxical situation of not being capable of calculating drag and flow separation over aerodynamic bodies because the dimensional analysis of the Navier–Stokes equations based on the same reference length in all directions seemed "to let the viscosity effect appear quite subordinate" with respect to the effect of inertia "almost always [...] in cases of fluid motion occurring in technology," to use Prandtl's own words.

Nevertheless, in case the above mentioned assumptions are deemed to be applicable, the *simplified* set of MFD equations (SMFD) can be obtained from the FMFD equations after some manipulation:

$$\frac{\partial \rho}{\partial t} + \nabla \cdot (\rho \boldsymbol{v}) = 0 \tag{11a}$$

$$\frac{\partial \rho \boldsymbol{v}}{\partial t} + \nabla \cdot \left[\left(p + \gamma M^2 S \frac{B^2}{2} \right) \bar{\boldsymbol{I}} + \rho \boldsymbol{v}\boldsymbol{v} - \gamma M^2 S \boldsymbol{B}\boldsymbol{B} \right] - \frac{\sqrt{\gamma} M}{Re} \nabla \cdot \boldsymbol{\tau} = 0 \tag{11b}$$

$$\frac{\partial (E_t)}{\partial t} + \nabla \cdot \left[\left(E_t + p + \gamma M^2 S \frac{B^2}{2} \right) \boldsymbol{v} - \gamma M^2 S (\boldsymbol{v} \cdot \boldsymbol{B}) \boldsymbol{B} \right] + \frac{\sqrt{\gamma} M}{Re} \nabla \cdot (\boldsymbol{J}_U - \boldsymbol{\tau} \cdot \boldsymbol{v}) = \frac{\sqrt{\gamma} M}{Re_m} \gamma M^2 S \{ (\nabla \times \boldsymbol{B}) \cdot [\boldsymbol{\lambda}_e^{-1} (\nabla \times \boldsymbol{B})] - \boldsymbol{B} \cdot \nabla \times [\boldsymbol{\lambda}_e^{-1} (\nabla \times \boldsymbol{B})] \} \tag{11c}$$

$$\frac{\partial \boldsymbol{B}}{\partial t} + \boldsymbol{B}(\nabla \cdot \boldsymbol{v}) + (\boldsymbol{v} \cdot \nabla)\boldsymbol{B} - \boldsymbol{v}(\nabla \cdot \boldsymbol{B}) - (\boldsymbol{B} \cdot \nabla)\boldsymbol{v} = -\frac{\sqrt{\gamma} M}{Re_m} \nabla \times [\boldsymbol{\lambda}_e^{-1} (\nabla \times \boldsymbol{B})] \tag{11d}$$

with

$$E_t = \left(\rho e_m + \gamma M^2 S \frac{B^2}{2} \right) \tag{12}$$

Depending on the magnitude of the similarity parameters appearing in Eqs. (11), a subset of *borderline conditions* for the SMFD equations can also be devised:

1) *Very Small Magnetic Force Number ($S \ll 1$)*: This is a trivial case where the MFD equations reduce to the Navier–Stokes equations. The electromagnetic field is not sufficiently strong to produce any significative effect on fluid dynamics.

2) *Low Magnetic Reynolds Number ($Re_m \ll 1$)*: Considering Eqs. (10), one can see that, if the magnetic Reynolds number is very small, then the arguments leading to the SMFD approximation becomes questionable, as those terms containing the electric-charge density may become important. In this case, however, other stronger hypotheses are usually made. The first one is based on the observation that, for small values of Re_m, the *induced* magnetic field is negligible, so that only the *applied* magnetic field is present. The second hypothesis states that the divergence of the electric current can be assumed to be equal to zero. In case of a *steady* applied magnetic field, the above mentioned assumptions lead to [1,8]:

$$\nabla \times \boldsymbol{E} = 0 \quad \text{as} \quad \frac{\partial \boldsymbol{B}_{\text{app}}}{\partial t} = 0 \tag{13a}$$

$$\nabla \cdot \boldsymbol{j} = 0 \tag{13b}$$

As Eq. (13a) holds, then it is possible to define an electric potential ϕ such that

$$\boldsymbol{E} = -\nabla \phi \tag{14}$$

Equations (13b) and (14) produce the following equation in ϕ:

$$\nabla \cdot [\boldsymbol{\lambda}_e (-\nabla \phi + \boldsymbol{v} \times \boldsymbol{B}_{\text{app}})] = 0 \tag{15}$$

Vector $\boldsymbol{B}_{\text{app}}$ is known, as it represents the imposed magnetic field, whereas the kinematic field can be computed solving the mass, momentum and energy balance equations, whose source terms are, in this case, rather weak:

$$\frac{\partial}{\partial t} \begin{bmatrix} \rho \\ \rho \boldsymbol{v} \\ \rho e_m \end{bmatrix} + \nabla \cdot \begin{bmatrix} \rho \boldsymbol{v} \\ \rho \boldsymbol{v}\boldsymbol{v} + p\bar{I} \\ (\rho e_m + p)\boldsymbol{v} \end{bmatrix} = \frac{\sqrt{\gamma} M}{Re} \nabla \cdot \begin{bmatrix} 0 \\ \boldsymbol{\tau} \\ \boldsymbol{\tau} \cdot \boldsymbol{v} - \boldsymbol{J}_U \end{bmatrix} + \sqrt{\gamma} M Q \begin{bmatrix} 0 \\ \boldsymbol{j} \times \boldsymbol{B}_{\text{app}} \\ \boldsymbol{j} \cdot \boldsymbol{E} \end{bmatrix} \tag{16}$$

Of course, it is clear that Eqs. (15) and (16) are coupled together. Care must be taken when using the low-Re_m SMFD model, as its limit of applicability is not known a priori for any flowfield configuration and the decision about its choice is based on the user's experience.

[‡]English translation available at http://naca.larc.nasa.gov/digidoc/report/tm/52/NACA-TM-452.PDF [cited 25 August 2006].

3) *Very Large Magnetic Reynolds Number ($Re_m \gg 1$)*: When $Re_m \to \infty$, then magnetic convection is overwhelming with respect to magnetic diffusion. In this case, the magnetic field and the fluid dynamics field are strongly coupled and they react instantaneously to their reciprocal variations. Fluid and magnetic field are "frozen" together [9], as if the induced currents would inhibit any relative motion of the fluid and the field. In these conditions, the SMFD assumptions can be safely applied to Eqs. (10) and one can focus the attention on Eqs. (11), where those terms containing Re_m disappear and the equations take the form:

$$\frac{\partial}{\partial t}\begin{bmatrix}\rho\\ \rho\boldsymbol{v}\\ \boldsymbol{B}\\ E_t\end{bmatrix}+\nabla\cdot\begin{bmatrix}\rho\boldsymbol{v}\\ \rho\boldsymbol{v}\boldsymbol{v}+\left(p+\gamma M^2 S\frac{B^2}{2}\right)\bar{\boldsymbol{I}}-\gamma M^2 S\boldsymbol{B}\boldsymbol{B}\\ \boldsymbol{v}\boldsymbol{B}-\boldsymbol{B}\boldsymbol{v}\\ \left(E_t+p+\gamma M^2 S\frac{B^2}{2}\right)\boldsymbol{v}-\gamma M^2 S(\boldsymbol{v}\cdot\boldsymbol{B})\boldsymbol{B}\end{bmatrix}=\frac{\sqrt{\gamma}M}{Re}\nabla\cdot\begin{bmatrix}0\\ \boldsymbol{\tau}\\ 0\\ \boldsymbol{\tau}\cdot\boldsymbol{v}-\boldsymbol{J}_U\end{bmatrix} \tag{17}$$

IV. Numerical Solution of the Full Magnetofluid Dynamics Equations

Attempts to numerically compute the FMFD equations are very scarce in the literature, if not completely absent. The nearest application, to the authors' knowledge, is related to the so-called *two-fluids plasma model*, which treats the plasma as a combination of electron and ion fluids coupled through the electromagnetic field [10,11]. Conversely, most numerical methods for computational magnetofluid dynamics are based on the SMFD model and have been developed following the guidelines coming from CFD methods, as it is demonstrated by the large number of publications where numerical procedures for CMFD are borrowed from different families of CFD methods [12–24].

A. Governing Equations

The nondimensional form of the full magnetofluid dynamics equations is given by Eqs. (10), where the chemical components mass balance equations, whose presence is fundamental for evaluating the mixture transport properties, have not been included just because they will not be used in view of the simplifications defined in the following.

Because the aim of this work is to develop numerical methods capable of coupling the Maxwell and the fluid dynamics equations, we decide to simplify Eqs. (10a–10e) using the following approximations:

$$Re \to \infty \qquad \text{inviscid flow} \tag{18a}$$

$$\rho_c = 0 \qquad \text{null electric charge density} \tag{18b}$$

$$\boldsymbol{\lambda}_e \equiv \lambda_e = \text{const} \qquad \text{constant and scalar electric conductivity} \tag{18c}$$

$$\boldsymbol{J}_Q = \lambda_e(\boldsymbol{E}+\boldsymbol{v}\times\boldsymbol{B}) \qquad \text{generalized Ohm law} \tag{18d}$$

Thus, Eqs. (10a–10e) are changed into

$$\frac{\partial\rho}{\partial t}+\nabla\cdot(\rho\boldsymbol{v})=0 \tag{19a}$$

$$\frac{\partial\rho\boldsymbol{v}}{\partial t}+\nabla\cdot(\rho\boldsymbol{v}\boldsymbol{v}+p\boldsymbol{I})=\sqrt{\gamma}MQ\boldsymbol{J}_Q\times\boldsymbol{B} \tag{19b}$$

$$\frac{\partial(\rho e_m)}{\partial t}+\nabla\cdot[(\rho e_m+p)\boldsymbol{v}]=\sqrt{\gamma}MQ\boldsymbol{J}_Q\cdot\boldsymbol{E} \tag{19c}$$

$$\frac{\partial\boldsymbol{B}}{\partial t}+\nabla\times\boldsymbol{E}=0 \tag{19d}$$

$$\frac{V_\infty^2}{c^2}\frac{\partial\boldsymbol{E}}{\partial t}-\gamma M^2\nabla\times\boldsymbol{B}=-\sqrt{\gamma}MRe_m\boldsymbol{J}_Q \tag{19e}$$

Note that the condition expressed by Eq. (18b) represents the same approximation made for obtaining the *simplified magnetofluid dynamics* equations. However, because the displacement-current term is retained in Eq. (19e), the mathematical nature of the *full magnetofluid dynamics equations* is preserved and the numerical method presented in Sec. IV.B can be easily extended to account for the electric-charge density.

As the numerical method presented here adopts a cell-centered finite volume discretization of the computational domain, we need to write Eqs. (19) in their integral form

$$\int_\mathcal{V}\frac{\partial\rho}{\partial t}\,\mathrm{d}V+\int_\mathcal{S}\rho\boldsymbol{v}\cdot\boldsymbol{n}\,\mathrm{d}S=0 \tag{20a}$$

$$\int_\mathcal{V}\frac{\partial\rho\boldsymbol{v}}{\partial t}\,\mathrm{d}V+\int_\mathcal{S}\rho\boldsymbol{v}\boldsymbol{v}\cdot\boldsymbol{n}\,\mathrm{d}S+\int_\mathcal{S}p\boldsymbol{I}\cdot\boldsymbol{n}\,\mathrm{d}S=\sqrt{\gamma}MQ\int_\mathcal{V}\boldsymbol{J}_Q\times\boldsymbol{B}\,\mathrm{d}V \tag{20b}$$

$$\int_\mathcal{V}\frac{\partial(\rho e_m)}{\partial t}\,\mathrm{d}V+\int_\mathcal{S}(\rho e_m+p)\boldsymbol{v}\cdot\boldsymbol{n}\,\mathrm{d}S=\sqrt{\gamma}MQ\int_\mathcal{V}\boldsymbol{J}_Q\cdot\boldsymbol{E}\,\mathrm{d}V \tag{20c}$$

$$\int_\mathcal{V}\frac{\partial\boldsymbol{B}}{\partial t}\,\mathrm{d}V+\int_\mathcal{S}\boldsymbol{n}\times\boldsymbol{E}\,\mathrm{d}S=0 \tag{20d}$$

$$\frac{V_\infty^2}{c^2}\int_\mathcal{V}\frac{\partial\boldsymbol{E}}{\partial t}\,\mathrm{d}V-\gamma M^2\int_\mathcal{S}\boldsymbol{n}\times\boldsymbol{B}\,\mathrm{d}S=-\sqrt{\gamma}MRe_m\int_\mathcal{V}\boldsymbol{J}_Q\,\mathrm{d}V \tag{20e}$$

Moreover, because attention is focused on one-dimensional flows, we reduce Eqs. (20) into:

$$\int_{x_1}^{x_2}\frac{\partial\boldsymbol{W}}{\partial t}\,\mathrm{d}x+\boldsymbol{F}_2-\boldsymbol{F}_1=\int_{x_1}^{x_2}\boldsymbol{\Omega}\,\mathrm{d}x \tag{21}$$

where

$$\boldsymbol{W} = \begin{vmatrix} \rho \\ \rho u \\ \rho v \\ \rho w \\ \rho e_m \\ B_y \\ B_z \\ E_y \\ E_z \end{vmatrix}; \qquad \boldsymbol{F} = \begin{vmatrix} \rho u \\ p + \rho uu \\ \rho vu \\ \rho wu \\ (\rho e_m + p)u \\ -E_z \\ E_y \\ \gamma M^2 \frac{c^2}{V_\infty^2} B_z \\ -\gamma M^2 \frac{c^2}{V_\infty^2} B_y \end{vmatrix} \tag{22}$$

$$\boldsymbol{\Omega} = \lambda_e \begin{vmatrix} 0 \\ \sqrt{\gamma} MQ[E_y B_z - E_z B_y + v B_x B_y + w B_x B_z - u(B_y^2 + B_z^2)] \\ \sqrt{\gamma} MQ[E_z B_x - E_x B_z + w B_y B_z + u B_y B_x - v(B_z^2 + B_x^2)] \\ \sqrt{\gamma} MQ[E_x B_y - E_y B_x + u B_z B_x + v B_z B_y - w(B_x^2 + B_y^2)] \\ \sqrt{\gamma} MQ[\|E\|^2 + E_x(vB_z - wB_y) + E_y(wB_x - uB_z) + E_z(uB_y - vB_x)] \\ 0 \\ 0 \\ \sqrt{\gamma} M \frac{c^2}{V_\infty^2} Re_m (E_y + wB_x - uB_z) \\ \sqrt{\gamma} M \frac{c^2}{V_\infty^2} Re_m (E_z + uB_y - vB_x) \end{vmatrix} \tag{23}$$

Note that the first five elements of vectors $\boldsymbol{W}$, $\boldsymbol{F}$ and $\boldsymbol{\Omega}$ refer to the fluid dynamics balance equations, whereas the last four are pertinent to electromagnetism. The coupling between the two phenomenologies occurs only through the source term, $\boldsymbol{\Omega}$, whereas in $\boldsymbol{W}$ and $\boldsymbol{F}$ the first five and the last four components are completely uncoupled.

At this stage, the mathematical model has been completely defined and it requires a numerical method for its solution.

B. Numerical Method

The major problem in the numerical simulation of the full magnetofluid dynamics equations resides in the fact that the signals propagation speeds typical of fluid dynamics differ orders of magnitude from the signal propagation speeds typical of electromagnetism. The former are of the order of the speed of sound, or at most 1 order of magnitude larger (flying at Mach 20 at high altitude, the fastest propagation speed is about 7000 m/s), whereas the latter are as fast as the speed of light (that is about 3×10^8 m/s). Because there are at least 5 orders of magnitude separating signal propagation speeds in fluid dynamics and in electromagnetism, the resulting coupled system is a very stiff one, and requires a special treatment.

Here, we want to solve the system of Eqs. (21–23) using a finite volume scheme. Solution methods for fluid dynamics and for electromagnetism, when considered separately, are well known [4]. However, the coupling requires that the two systems are solved simultaneously. Stability considerations request that, using explicit schemes, the common time step be very small, namely of the order of $\Delta x/c$. This is definitely a too small time step for efficient fluid dynamics computations. The way to overcome such an obstacle is to solve the Maxwell equations using implicit schemes, that allow for large computational time steps as they are nominally unconditionally stable. The fact that the speed of light is a constant parameter implies that the homogeneous electromagnetic part of the FMFD system has linear eigenvalues, so that the application of implicit schemes to the Maxwell equations allows for very large time steps (comparatively to the Maxwell system). Thus, one can conceive to march the fluid dynamics system in time for one iteration using the values of the electromagnetic field variables frozen at the beginning of the time step, and then to march the electromagnetics system in time for one iteration until the same time value of the companion fluid dynamics step is reached. In this second step, one can decide to use the flowfield values frozen at the beginning of the fluid dynamics time step, or those obtained at the end of it, or an average value. Clearly, such a way of proceeding does not possess the time resolution necessary to resolve electromagnetic phenomena that evolve with very high frequency, even though, in principle, the method permits to reduce the electromagnetic step at will.

Another delicate point arises when source terms become large. In fact, it is well known that the numerical solution of hyperbolic equations becomes very hard when stiff source terms are present. Such a problem is typical, for instance, of the numerical simulation of chemically reacting flows. In the full MFD equations, source terms become stiff when the magnetic Reynolds number is large. To increase the value of Re_m above which the numerical method fails, the classical strategy of implicitly treating the source terms can be used.

Putting into practice what we just anticipated results in the development of a two-steps numerical procedure. In the first step, the fluid dynamic part of the equations is solved using a second order explicit integration scheme for the homogeneous part and an implicit procedure for the source term. During this step, the electromagnetic variables are considered as frozen. Indicating with $\boldsymbol{W}^f$, $\boldsymbol{F}^f$ and $\boldsymbol{\Omega}^f$ that parts of $\boldsymbol{W}$, $\boldsymbol{F}$ and $\boldsymbol{\Omega}$ pertinent to the fluid dynamics equations, we write

$$\frac{\tilde{\Delta} \boldsymbol{W}_N^f}{\tilde{\Delta} t} \Delta x + (\boldsymbol{F}_{N+\frac{1}{2}}^f)^K - (\boldsymbol{F}_{N-\frac{1}{2}}^f)^K = (\boldsymbol{\Omega}_N^f)^{K+\frac{1}{2}} \Delta x = (\boldsymbol{\Omega}_N^f)^K \Delta x + \left[\left(\frac{\partial \boldsymbol{\Omega}_N^f}{\partial \boldsymbol{W}_N^f} \right)^K \frac{\Delta \boldsymbol{W}_N^f}{\tilde{\Delta} t} \frac{\tilde{\Delta} t}{2} \right] \Delta x \tag{24}$$

where

$$\frac{\partial \boldsymbol{\Omega}_N^f}{\partial \boldsymbol{W}_N^f} = \sqrt{\gamma} MQ \lambda_e \begin{bmatrix} 0 & 0 & 0 & 0 & 0 \\ -\frac{(\boldsymbol{v}\times\boldsymbol{B})_x}{\rho} & -\frac{B_y^2 + B_z^2}{\rho} & \frac{B_x B_y}{\rho} & \frac{B_x B_z}{\rho} & 0 \\ -\frac{(\boldsymbol{v}\times\boldsymbol{B})_y}{\rho} & \frac{B_y B_x}{\rho} & -\frac{B_x^2 + B_z^2}{\rho} & \frac{B_y B_z}{\rho} & 0 \\ -\frac{(\boldsymbol{v}\times\boldsymbol{B})_z}{\rho} & \frac{B_z B_x}{\rho} & \frac{B_z B_y}{\rho} & -\frac{B_x^2 + B_y^2}{\rho} & 0 \\ -\frac{(\boldsymbol{v}\times\boldsymbol{B})\cdot\boldsymbol{E}}{\rho} & -\frac{(\boldsymbol{E}\times\boldsymbol{B})_x}{\rho} & -\frac{(\boldsymbol{E}\times\boldsymbol{B})_y}{\rho} & -\frac{(\boldsymbol{E}\times\boldsymbol{B})_z}{\rho} & 0 \end{bmatrix} \tag{25}$$

In this paper, any Jacobian matrix will be meant to be computed at time step K. Therefore, from now on, we will omit the superscript K when writing such terms.

It is clear from Eqs. (24) and (25) that the mass balance equation, which has no source term, can be solved separately from the others:

$$\rho_N^{K+1} = \rho_N^K - \{\Delta F^\rho\}\frac{\tilde{\Delta}t}{\Delta x} \tag{26}$$

Conversely, the momentum and energy balance equations are coupled through the source terms, whose implicit integration results in the system:

$$\frac{\tilde{\Delta}\hat{\boldsymbol{W}}_N^f}{\tilde{\Delta}t}\Delta x + (\hat{\boldsymbol{F}}^f_{N+\frac{1}{2}})^K - (\hat{\boldsymbol{F}}^f_{N-\frac{1}{2}})^K = (\hat{\boldsymbol{\Omega}}_N^f)^K\Delta x + \left[\frac{\partial\hat{\boldsymbol{\Omega}}_N^f}{\partial\rho_N}\frac{\tilde{\Delta}\rho_N}{\tilde{\Delta}t}\frac{\tilde{\Delta}t}{2}\right]\Delta x + \left[\frac{\partial\hat{\boldsymbol{\Omega}}_N^f}{\partial\hat{\boldsymbol{W}}_N^f}\frac{\Delta\hat{\boldsymbol{W}}_N^f}{\tilde{\Delta}t}\frac{\tilde{\Delta}t}{2}\right]\Delta x \tag{27}$$

The sign $\hat{}$ above vectors $\boldsymbol{W}^f$, $\boldsymbol{F}^f$ and $\boldsymbol{\Omega}^f$ indicates that the mass balance equations is excluded from Eq. (27).

The solution of Eq. (27) requires the inversion of a (4×4) matrix for each computational cell:

$$[\boldsymbol{A}]_N\tilde{\Delta}\hat{\boldsymbol{W}}_N^f = -(\Delta\hat{\boldsymbol{F}}_N^f)^K\frac{\tilde{\Delta}t}{\Delta x} + (\hat{\boldsymbol{\Omega}}_N^f)^K\Delta t + \frac{\partial\hat{\boldsymbol{\Omega}}_N^f}{\partial\rho_N}\tilde{\Delta}\rho_N\frac{\tilde{\Delta}t}{2} \tag{28}$$

where

$$[\boldsymbol{A}]_N = \begin{bmatrix} 1+C^f\frac{B_y^2+B_z^2}{\rho}\frac{\tilde{\Delta}t}{2} & -C^f\frac{B_xB_y}{\rho}\frac{\tilde{\Delta}t}{2} & -C^f\frac{B_xB_z}{\rho}\frac{\tilde{\Delta}t}{2} & 0\\ -C^f\frac{B_yB_x}{\rho}\frac{\tilde{\Delta}t}{2} & 1+C^f\frac{B_x^2+B_z^2}{\rho}\frac{\tilde{\Delta}t}{2} & -C^f\frac{B_yB_z}{\rho}\frac{\tilde{\Delta}t}{2} & 0\\ -C^f\frac{B_zB_x}{\rho}\frac{\tilde{\Delta}t}{2} & -C^f\frac{B_zB_y}{\rho}\frac{\tilde{\Delta}t}{2} & 1+C^f\frac{B_x^2+B_y^2}{\rho}\frac{\tilde{\Delta}t}{2} & 0\\ C^f\frac{(\boldsymbol{E}\times\boldsymbol{B})_x}{\rho}\frac{\tilde{\Delta}t}{2} & C^f\frac{(\boldsymbol{E}\times\boldsymbol{B})_y}{\rho}\frac{\tilde{\Delta}t}{2} & C\frac{(\boldsymbol{E}\times\boldsymbol{B})_z}{\rho}\frac{\tilde{\Delta}t}{2} & 1\end{bmatrix} \tag{29}$$

with

$$C^f = \sqrt{\gamma}MQ\lambda_e \tag{30}$$

The elements of $[\boldsymbol{A}]_N$ must be computed using the local values of $\boldsymbol{B}$, $\boldsymbol{E}$, and $\boldsymbol{v}$ at each N cell. Note that, because the time variation of density $\tilde{\Delta}\rho$ is already known from Eq. (26), the derivatives with respect to density that are present in the source term components are treated explicitly in Eq. (27), with

$$\frac{\partial\hat{\boldsymbol{\Omega}}_N^f}{\partial\rho_N} = C^f\left[-\frac{(\boldsymbol{v}\times\boldsymbol{B})_x}{\rho}, -\frac{(\boldsymbol{v}\times\boldsymbol{B})_y}{\rho}, -\frac{(\boldsymbol{v}\times\boldsymbol{B})_z}{\rho}, -\frac{(\boldsymbol{v}\times\boldsymbol{B})\cdot\boldsymbol{E}}{\rho}\right]^T \tag{31}$$

At this point, the only missing information concerns the way in which fluxes $\boldsymbol{F}^f$ are computed. In this work, such an operation is carried out using an upwind flux-difference splitting method widely used by the first author for computing high speed flows [25,26].

Once fluid dynamics variables have been computed as described above, the second step consists in solving the electromagnetic part of the equations system. In this case, the integration scheme is fully implicit, in such a way that the same time-integration interval of fluid dynamics $\tilde{\Delta}t$ can be used without running into stability problems. Fluid dynamics variables are treated as if they were frozen at the values obtained after the first step of the procedure. Therefore, the integration scheme for the electromagnetic part of the FMFD equations (i.e., the Maxwell equations) is

$$\frac{\tilde{\Delta}\boldsymbol{W}_N^m}{\tilde{\Delta}t}\Delta x + (\boldsymbol{F}^m_{N+\frac{1}{2}})^{K+1} - (\boldsymbol{F}^m_{N-\frac{1}{2}})^{K+1} = (\boldsymbol{\Omega}_N^m)^{K+\frac{1}{2}}\Delta x \tag{32}$$

Assuming that the fluxes at each cell interface depend on the two neighboring cells only, Eq. (32) can be expanded as

$$\frac{\tilde{\Delta}\boldsymbol{W}_N^m}{\tilde{\Delta}t}\Delta x + (\boldsymbol{F}^m_{N+\frac{1}{2}})^K + \frac{\partial\boldsymbol{F}^m_{N+\frac{1}{2}}}{\partial\boldsymbol{W}^m_{N+1}}\frac{\tilde{\Delta}\boldsymbol{W}^m_{N+1}}{\tilde{\Delta}t}\frac{\tilde{\Delta}t}{2} + \frac{\partial\boldsymbol{F}^m_{N+\frac{1}{2}}}{\partial\boldsymbol{W}^m_N}\frac{\tilde{\Delta}\boldsymbol{W}^m_N}{\tilde{\Delta}t}\frac{\tilde{\Delta}t}{2} - (\boldsymbol{F}^m_{N-\frac{1}{2}})^K - \frac{\partial\boldsymbol{F}^m_{N-\frac{1}{2}}}{\partial\boldsymbol{W}^m_N}\frac{\tilde{\Delta}\boldsymbol{W}^m_N}{\tilde{\Delta}t}\frac{\tilde{\Delta}t}{2} - \frac{\partial\boldsymbol{F}^m_{N-\frac{1}{2}}}{\partial\boldsymbol{W}^m_{N-1}}\frac{\tilde{\Delta}\boldsymbol{W}^m_{N-1}}{\tilde{\Delta}t}\frac{\tilde{\Delta}t}{2} = (\boldsymbol{\Omega}_N^m)^K\Delta x + \left[\frac{\partial\boldsymbol{\Omega}^m_N}{\partial\boldsymbol{W}^m_N}\frac{\tilde{\Delta}\boldsymbol{W}^m_N}{\tilde{\Delta}t}\frac{\tilde{\Delta}t}{2}\right]\Delta x \tag{33}$$

As the homogenous part of the Maxwell equations does not provide for the presence of discontinuities, a centered scheme can be used to evaluate the elements of $\boldsymbol{F}^m$ at each cell interface without the need of introducing any "ad hoc" artificial dissipation:

$$\boldsymbol{F}^m_{N\pm\frac{1}{2}} = \tfrac{1}{2}(\boldsymbol{F}^m_N + \boldsymbol{F}^m_{N\pm1}) \tag{34}$$

The solution of Eq. (33) requires the inversion of a block tridiagonal matrix $[\boldsymbol{D}]$ across the whole computational domain. The linear system to be solved is

$$[\boldsymbol{D}]\{\tilde{\Delta}\boldsymbol{W}^m\} = -\{\Delta\boldsymbol{F}^m\}\frac{\tilde{\Delta}t}{\Delta x} + \{\boldsymbol{\Omega}^m\}\tilde{\Delta}t \tag{35}$$

As anticipated, matrix $[\boldsymbol{D}]$ is a block tridiagonal matrix. If Eq. (34) is used to compute $\boldsymbol{F}^m$, then the subdiagonal blocks $[\boldsymbol{L}]$, the superdiagonal blocks $[\boldsymbol{R}]$ and diagonal blocks $[\boldsymbol{C}]$ have the form

$$[\boldsymbol{L}] = \begin{bmatrix} 0 & 0 & 0 & \frac{1}{2}\frac{\tilde{\Delta}t}{\Delta x}\\ 0 & 0 & -\frac{1}{2}\frac{\tilde{\Delta}t}{\Delta x} & 0\\ 0 & -\frac{K}{2}\frac{\tilde{\Delta}t}{\Delta x} & 0 & 0\\ \frac{K}{2}\frac{\tilde{\Delta}t}{\Delta x} & 0 & 0 & 0\end{bmatrix};$$
$$[\boldsymbol{R}] = \begin{bmatrix} 0 & 0 & 0 & -\frac{1}{2}\frac{\tilde{\Delta}t}{\Delta x}\\ 0 & 0 & \frac{1}{2}\frac{\tilde{\Delta}t}{\Delta x} & 0\\ 0 & \frac{K}{2}\frac{\tilde{\Delta}t}{\Delta x} & 0 & 0\\ -\frac{K}{2}\frac{\tilde{\Delta}t}{\Delta x} & 0 & 0 & 0\end{bmatrix} \tag{36}$$
$$[\boldsymbol{C}] = \begin{bmatrix} 1 & 0 & 0 & 0\\ 0 & 1 & 0 & 0\\ 0 & -C^m u_N\frac{\tilde{\Delta}t}{2} & 1+C^m\frac{\tilde{\Delta}t}{2} & 0\\ C^M u_N\frac{\tilde{\Delta}t}{2} & 0 & 0 & 1+C^m\frac{\tilde{\Delta}t}{2}\end{bmatrix}$$

where

$$K = \gamma M^2\frac{c^2}{V_\infty^2} \tag{37}$$

$$C^m = \sqrt{\gamma}M\frac{c^2}{V_\infty^2}Re_m\lambda_e \tag{38}$$

At the boundaries of the computational domain, the form of $[\boldsymbol{L}]$, $[\boldsymbol{R}]$, and $[\boldsymbol{C}]$ will change according to the enforced boundary conditions.

1. Accuracy

The fluid dynamic part of the FMFD equations is computed reconstructing the convective fluxes with a second order scheme of the essentially nonoscillatory (ENO) family [27], as described in [26]. In addition, source terms are computed at the intermediate time step $K+1/2$ with an implicit scheme. Thus, the numerical method for the fluid dynamic step has a nominal second order accuracy both in space and in time.

The Maxwell equations are solved using central differences for computing the fluxes, which, therefore, are second order accurate in space. The integration in time is performed with an implicit evaluation of the fluxes at the electromagnetic time step $K+1$,

whereas source terms are evaluated at the intermediate electromagnetic time step $K+\frac{1}{2}$.

V. Numerical Solution of the Simplified Magnetofluid Dynamics Equations

Numerical methods for the simplified MFD equations can be different depending on the magnetic Reynolds number of the application. In the limit of *very small* magnetic Reynolds numbers, the SMFD equations could be further modified and the so-called *Low-Re_m SMFD equations* are obtained [8]. In the latter case, considerable simplification is introduced by noting that the induced magnetic field is negligible and the Ampere's law is discarded. Conversely, in the general SMFD formulation, no assumption is made on the magnetic Reynolds number and the magnetic induction equation is explicitly solved to obtain the induced magnetic field.

Most numerical methods for solving the general formulation of the SMFD equations in compressible flow conditions adopt upwind schemes originally developed for the *ideal magnetohydrodynamics (MHD)* equations, that is the homogenous and inviscid part of the SMFD equations. The approach replicates the one followed by numerical methods for compressible flows: first upwind schemes were developed for the Euler equations in one-dimension and then extended to two and three-dimensions and to Navier–Stokes. Upwind methods developed to solve the ideal MHD equations belong to the Roe family [14–16], to the flux-vector splitting (FVS) family [17], to the Harten–Lax–van Leer– Einfeldt (HLLE) family [18,19], to the gas-kinetics theory based flux-vector splitting family [20], to the piecewise parabolic method (PPM) family [21], to the Lax–Friedrichs family [22] and to the Osher family [28]. With the exception of the gas-kinetic FVS method, all the above cited upwind methods follow the Godunov approach and thus necessitate knowledge of the eigenvectors and eigenvalues system that characterize the one-dimensional ideal MHD equations. Other numerical methods for MHD adopt the total-variation diminishing (TVD) scheme [23] or a combination of compact-difference for space derivatives and the classical Runge–Kutta method for time derivatives [24]. A numerical technique for solving such a classical form of the SMFD equations will be discussed in Sec. V.A.

A second possibility consists in solving the SMFD equations using numerical methods conceived for compressible fluid dynamics as far as mass, momentum, and energy balance equations are concerned and treating the magnetic induction equation in a separate fashion. Such a technique, which will be introduced in Sec. V.B, is particularly well suited for cases where the magnetic Reynolds number ranges from low to moderate values.

As a final remark, it should be also emphasized that, when such methods are extended to more than one dimension, special procedures must be adopted to enforce the $\nabla\cdot\boldsymbol{B}=0$ constraint in the integration of the discretized equations [17,29–33]. In one dimension, enforcing the condition $B_x=\text{const}$ automatically satisfies the constraint.

A. Classical Numerical Solution of the Simplified Magnetofluid Dynamics Equations

Formally, it is possible to write the SMFD equations in different forms that, despite having exactly the same physical meaning, lead to different numerical methodologies. In a first case, one can decide to maintain the fluid dynamics fluxes as distinct with respect to the electromagnetic terms in the momentum and energy balance equations. Such a choice makes it possible to solve the mass, momentum, and energy balance equations using normal CFD techniques for compressible flows (with the addition of magnetic source terms) and the magnetic induction equation using an implicit centered scheme. Such a formalism and the related numerical method is particularly suitable for those cases where the magnetic Reynolds number is not excessively large, but where magnetic induction cannot be neglected. In the second case, it is possible to write the equations system in divergence form with the addition of *magnetic* source terms that appear only in the magnetic induction and energy equations and that depend on the magnetic Reynolds number [Eqs. (11)]. Those fluxes that appear under the divergence operator and that are not related to momentum and energy diffusion are composed of a fluid dynamics part and of a part related to the magnetic field. Thus, there can be in general a very strict coupling between the flowfield and the magnetic field. The mutual adaptation of the one to the other is controlled by the ratio between convection and magnetic diffusion effects, which is represented by the magnitude of the *magnetic Reynolds number*. In this case, the numerical technique is derived from the numerical methods for MHD flows, with the addition of *resistive* source terms. Such a formulation fits well in those cases where the magnetic Reynolds number is quite large.

1. Governing Equations

The most popular form of the *simplified magnetofluid dynamics (SMFD)* equations is given by Eqs. (11). Neglecting momentum and energy transport, Eqs. (11) can be rewritten in integral form as follows:

$$\int_{\mathcal{V}}\frac{\partial \boldsymbol{W}^s}{\partial t}\,\mathrm{d}V+\int_{\mathcal{S}}\boldsymbol{F}^s\cdot\boldsymbol{n}\,\mathrm{d}S=\int_{\mathcal{V}}\boldsymbol{\Omega}^s\,\mathrm{d}V \tag{39}$$

where

$$\boldsymbol{W}^s=\begin{vmatrix}\rho\\ \rho\boldsymbol{v}\\ \boldsymbol{B}\\ E_t\end{vmatrix};\qquad \boldsymbol{F}^s=\begin{vmatrix}\rho\boldsymbol{v}\\ \rho\boldsymbol{v}\boldsymbol{v}+\left(p+\gamma M^2S\frac{B^2}{2}\right)\bar{\boldsymbol{I}}-\gamma M^2S\boldsymbol{B}\boldsymbol{B}\\ \boldsymbol{v}\boldsymbol{B}-\boldsymbol{B}\boldsymbol{v}\\ \left(E_t+p+\gamma M^2S\frac{B^2}{2}\right)\boldsymbol{v}-\gamma M^2S(\boldsymbol{v}\cdot\boldsymbol{B})\boldsymbol{B}\end{vmatrix} \tag{40}$$

and

$$\boldsymbol{\Omega}^s=\begin{vmatrix}0\\ \boldsymbol{0}\\ -\frac{\sqrt{\gamma}M}{Re_m}\nabla\times\left(\frac{\nabla\times\boldsymbol{B}}{\lambda_e}\right)\\ \frac{\sqrt{\gamma}M}{Re_m}\gamma M^2S\frac{1}{\lambda_e}[(\nabla\times\boldsymbol{B})^2+\boldsymbol{B}\cdot\nabla^2\boldsymbol{B}]\end{vmatrix} \tag{41}$$

If we restrict our model to one-dimension, we remain with the following system of equations:

$$\int_{x_1}^{x_2}\frac{\partial \boldsymbol{W}^s}{\partial t}\,\mathrm{d}x+\boldsymbol{F}_2^s-\boldsymbol{F}_1^s=\int_{x_1}^{x_2}\boldsymbol{\Omega}^s\,\mathrm{d}x \tag{42}$$

where

$$\boldsymbol{W}^s=\begin{vmatrix}\rho\\ \rho u\\ \rho v\\ \rho w\\ B_y\\ B_z\\ E_t\end{vmatrix}$$

$$\boldsymbol{F}^s=\begin{vmatrix}\rho u\\ \rho uu+p+\gamma M^2S\frac{B^2}{2}-\gamma M^2SB_xB_x\\ \rho vu-\gamma M^2SB_yB_x\\ \rho wu-\gamma M^2SB_zB_x\\ B_yu-vB_x\\ B_zu-wB_x\\ \left(E_t+p+\gamma M^2S\frac{B^2}{2}\right)u-\gamma M^2S(uB_x+vB_y+wB_z)B_x\end{vmatrix} \tag{43}$$

Table 1 Left and right states of the initial discontinuity for the considered Riemann problem

	ρ [kg/m^3]	p [Pa]	u [m/s]	v [m/s]	w [m/s]	B_x [T]	B_y [T]	B_z [T]
Left side	12.25	1×10^6	0.0	0.0	0.0	0.75	1.0	0.0
Right side	1.225	1×10^5	0.0	0.0	0.0	0.75	1.0	0.0

Table 2 Similarity parameters pertinent to the reference values of Table 3

S	Re_m/λ_e [Ohm·m]	Q/λ_e [Ohm·m]	M	$\gamma M^2 S$	$\sqrt{\gamma}M/(Re_m/\lambda_e)$ [mho/m]	V_∞/c
0.714	4.24×10^{-4}	3.03×10^{-4}	1.0	1.0	2789.01	1.127×10^{-6}

and

$$\boldsymbol{\Omega}^{s} = \frac{1}{\lambda_e} \begin{vmatrix} 0 \\ 0 \\ 0 \\ 0 \\ \frac{\sqrt{\gamma}M}{Re_m}\left(\frac{\partial^2 B_y}{\partial x^2}\right) \\ \frac{\sqrt{\gamma}M}{Re_m}\left(\frac{\partial^2 B_z}{\partial x^2}\right) \\ \frac{\sqrt{\gamma}M}{Re_m}\gamma M^2 S\left[\left(\frac{\partial B_y}{\partial x}\right)^2 + \left(\frac{\partial B_z}{\partial x}\right)^2 + B_y\frac{\partial^2 B_y}{\partial x^2} + B_z\frac{\partial^2 B_z}{\partial x^2}\right] \end{vmatrix} \tag{44}$$

The electric field $\boldsymbol{E}$ can be computed from the relation:

$$\boldsymbol{E} = \frac{\sqrt{\gamma}M}{Re_m}\frac{1}{\lambda_e}\nabla \times \boldsymbol{B} - \boldsymbol{v} \times \boldsymbol{B} \tag{45}$$

The electric-charge density, ρ_c does not appear in Eqs. (42–44), but, in general, it can be reconstructed from the Gauss law for electricity:

$$\rho_c = \varepsilon_0 \nabla \cdot \boldsymbol{E} \tag{46}$$

Enforcing the magnetohydrodynamic approximation completely changes the mathematical nature of the MFD equations. The propagation of electromagnetic signals with the speed of light is completed removed and the homogenous SMFD system (that is in the limit of infinite viscous and magnetic Reynolds numbers) is characterized by eigenvalues and eigenvectors that correspond to seven different signals with the respective propagation speeds. Details on the subject are given in [28] and are widely reported in the literature [5,34,35].

2. *Numerical Method*

Here, we present a numerical method conceived for the general formulation of the SMFD equations, which is based on the upwind solver presented in [28]. The integration of the equations system is carried out in an explicit fashion as far as the convective part is concerned. In addition, source terms are computed with an implicit scheme to overcome stability problems that may occur for small values of the magnetic Reynolds number, when the source term becomes very large. In fact, the system contained in Eqs. (39–41) presents source terms that become large for small values of Re_m and therefore its numerical solution may encounter severe difficulties in such a regime.

We start our description of the method with discretizing the one-dimensional SMFD equations using a cell-centered finite volume approximation:

$$\frac{\tilde{\Delta}\boldsymbol{W}^s}{\tilde{\Delta}t}\Delta x + \boldsymbol{F}^{sK}_{N+\frac{1}{2}} - \boldsymbol{F}^{sK}_{N-\frac{1}{2}} = \boldsymbol{\Omega}^{sK+\frac{1}{2}}_N \Delta x \tag{47}$$

The first four equations contained in the system of Eq. (47), namely the mass and momentum balance equations, have no source term and they can be solved using a standard explicit scheme:

$$\tilde{\Delta}W^i_N = -\frac{\tilde{\Delta}t}{\Delta x}\Delta F^i_N \tag{48}$$

Conversely, the magnetic induction equations and the total energy balance equation are characterized by the presence of source terms, whose implicit integration provides that they be computed at time step $K + \frac{1}{2}$. In this work, the space derivatives of the magnetic field contained in the source terms are computed according to the formulas:

$$\frac{\partial B_i}{\partial x} \approx \frac{[d_1(B_i)_{N+1} + d_2(B_i)_N + d_3(B_i)_{N-1}]}{\Delta x} \tag{49a}$$

$$\frac{\partial^2 B_i}{\partial x^2} \approx \frac{[l_1(B_i)_{N+1} + l_2(B_i)_N + l_3(B_i)_{N-1}]}{\Delta x^2} \tag{49b}$$

where, for internal points, we use

$$d_1 = \tfrac{1}{2} \qquad d_2 = 0 \qquad d_3 = -\tfrac{1}{2} \tag{50a}$$

$$l_1 = 1 \qquad l_2 = -2 \qquad l_3 = 1 \tag{50b}$$

whereas other coefficients have to be adopted for any particular boundary condition. Thus, the source terms depend not only on the values of $\boldsymbol{B}$ at the local mesh point, but also at the two neighboring cells:

$$\boldsymbol{\Omega}^{sK+\frac{1}{2}}_N = \boldsymbol{\Omega}^{sK}_N + \left[\frac{\partial \boldsymbol{\Omega}^s_N}{\partial \boldsymbol{W}^s_{N-1}}\frac{\tilde{\Delta}\boldsymbol{W}^s_{N-1}}{\tilde{\Delta}t} + \frac{\partial \boldsymbol{\Omega}^s_N}{\partial \boldsymbol{W}^s_N}\frac{\tilde{\Delta}\boldsymbol{W}^s_N}{\tilde{\Delta}t} + \frac{\partial \boldsymbol{\Omega}^s_N}{\partial \boldsymbol{W}^s_{N+1}}\frac{\tilde{\Delta}\boldsymbol{W}^s_{N+1}}{\tilde{\Delta}t}\right]\frac{\tilde{\Delta}t}{2} \tag{51}$$

Table 3 Characteristic reference values

ρ_0 [kg/m^3]	p_0 [Pa]	V_0 [m/s]	V_∞ [m/s]	B_0 [T]	L
1.225	1×10^5	285.71429	338.06169	0.35424929	1.0

Table 4 Extension of the computational domain as a function of the electrical conductivity. *Lb* and *Rb* stand for left and right boundary, respectively. The initial discontinuity is always placed at $x/L = 0.5$

λ_e [S/m]	δ_{B_y}/L	$(x/L)_{\mathrm{Lb}}$	$(x/L)_{\mathrm{Rb}}$
1.0×10^6	0.0941	0.0	1.0
1.0×10^5	0.2980	−0.5	1.5
1.0×10^4	0.9410	−1.5	2.5
1.0×10^3	2.9800	−3.5	4.5
1.0×10^2	9.4100	−11.5	12.5
1.0×10^0	94.1000	−99.5	100.5

Note that the source terms in the two magnetic induction equations are uncoupled, so that those equations can be solved separately. In general, for each component of the magnetic induction equation, it will be necessary to solve a system that requires the inversion of a tridiagonal matrix whose rank is equal to the number of cells:

$$[\boldsymbol{T}]\{\tilde{\Delta}B_i\} = -\{F^{B_i}\}\frac{\tilde{\Delta}t}{\Delta x} + \{\Omega^{B_i}\}\tilde{\Delta}t \tag{52}$$

The elements of the tridiagonal matrix, $[\boldsymbol{T}]$, are

$$a = -\frac{\partial(\Omega^{B_i})_N}{\partial(B_i)_{N-1}}\frac{\tilde{\Delta}t}{2} = -\frac{\sqrt{\gamma}M}{Re_m}\frac{1}{\lambda_e}\frac{l_3}{\Delta x^2}\frac{\tilde{\Delta}t}{2} \qquad \text{subdiagonal term} \tag{53a}$$

$$b = 1 - \frac{\partial(\Omega^{B_i})_N}{\partial(B_i)_N}\frac{\tilde{\Delta}t}{2} = 1 - \frac{\sqrt{\gamma}M}{Re_m}\frac{1}{\lambda_e}\frac{l_2}{\Delta x^2}\frac{\tilde{\Delta}t}{2} \qquad \text{diagonal term} \tag{53b}$$

$$c = -\frac{\partial(\Omega^{B_i})_N}{\partial(B_i)_{N+1}}\frac{\tilde{\Delta}t}{2} = -\frac{\sqrt{\gamma}M}{Re_m}\frac{1}{\lambda_e}\frac{l_1}{\Delta x^2}\frac{\tilde{\Delta}t}{2} \qquad \text{superdiagonal term} \tag{53c}$$

In addition, the half-implicit discretization of the total energy balance equation does not require the inversion of a matrix, because the source term component Ω^{E_t} only depends from the space derivatives of $\boldsymbol{B}$. Thus, we can solve for $\{\tilde{\Delta}E_t\}$ using the equation

$$\tilde{\Delta}E_{tN} + \Delta F_N^{E_t}\frac{\tilde{\Delta}t}{\Delta x} = (\Omega_N^{E_t})^K\tilde{\Delta}t + \left[\sum_{i=y,z}\frac{\partial\Omega_N^{E_t}}{\partial B_{iN-1}}\tilde{\Delta}B_{iN-1} + \sum_{i=y,z}\frac{\partial\Omega_N^{E_t}}{\partial B_{iN}}\tilde{\Delta}B_{iN} + \sum_{i=y,z}\frac{\partial\Omega_N^{E_t}}{\partial B_{iN+1}}\tilde{\Delta}B_{iN+1}\right]\frac{\tilde{\Delta}t}{2} \tag{54}$$

with

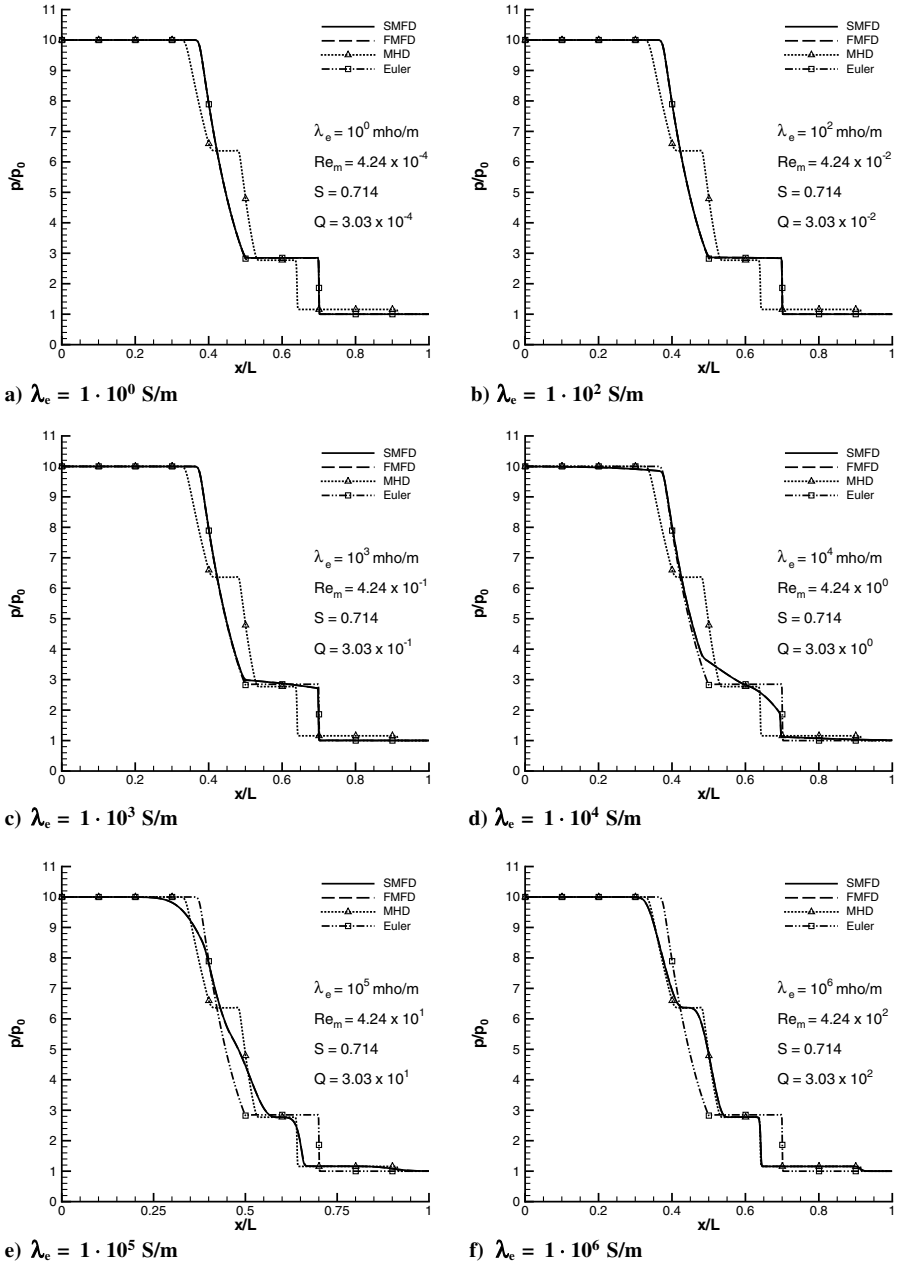

a) $\lambda_e = 1 \cdot 10^0$ S/m b) $\lambda_e = 1 \cdot 10^2$ S/m

c) $\lambda_e = 1 \cdot 10^3$ S/m d) $\lambda_e = 1 \cdot 10^4$ S/m

e) $\lambda_e = 1 \cdot 10^5$ S/m f) $\lambda_e = 1 \cdot 10^6$ S/m

Fig. 2 Pressure plots obtained using different values of λ_e in the considered shock-tube problem.

$$\frac{\partial \Omega_N^{E_i}}{\partial B_{iN-1}} = \frac{\sqrt{\gamma}M}{Re_m}\gamma M^2 S \frac{1}{\lambda_e}\left[2\left(\frac{\partial B_i}{\partial x}\right)_N \frac{d_3}{\Delta x} + B_i \frac{l_3}{\Delta x^2}\right] \tag{55a}$$

$$\frac{\partial \Omega_N^{E_i}}{\partial B_{iN}} = \frac{\sqrt{\gamma}M}{Re_m}\gamma M^2 S \frac{1}{\lambda_e}\left[2\left(\frac{\partial B_i}{\partial x}\right)_N \frac{d_2}{\Delta x} + B_i \frac{l_2}{\Delta x^2} + \left(\frac{\partial^2 B_i}{\partial x^2}\right)_N\right] \tag{55b}$$

$$\frac{\partial \Omega_N^{E_i}}{\partial B_{iN+1}} = \frac{\sqrt{\gamma}M}{Re_m}\gamma M^2 S \frac{1}{\lambda_e}\left[2\left(\frac{\partial B_i}{\partial x}\right)_N \frac{d_1}{\Delta x} + B_i \frac{l_1}{\Delta x^2}\right] \tag{55c}$$

In Eq. (54), all the increments $\{\tilde{\Delta}B_y\}$ and $\{\tilde{\Delta}B_z\}$ are known values previously obtained from the solution of Eq. (52).

3. Accuracy

An ENO reconstruction [27] and the use of the minmod limiter provide a reconstruction of the initial data for the computation of the convective fluxes that leads to a second order of accuracy in space. Second order of accuracy in time is achieved by adding a further correction to these values to account for the time dependency of the solution. In addition, source terms are computed at the intermediate step $K + \frac{1}{2}$ and the partial derivatives appearing in them are evaluated using finite difference formulas that are also second order accurate. Thus, globally, the numerical method for the SMFD equations has a nominal second order accuracy both in space and in time.

B. Loosely Coupled Numerical Solution of the Simplified Magnetofluid Dynamics Equations

In Sec. VII.D.1 it will be shown that the MHD solver on which the numerical solution of the SMFD equations is based may lead to

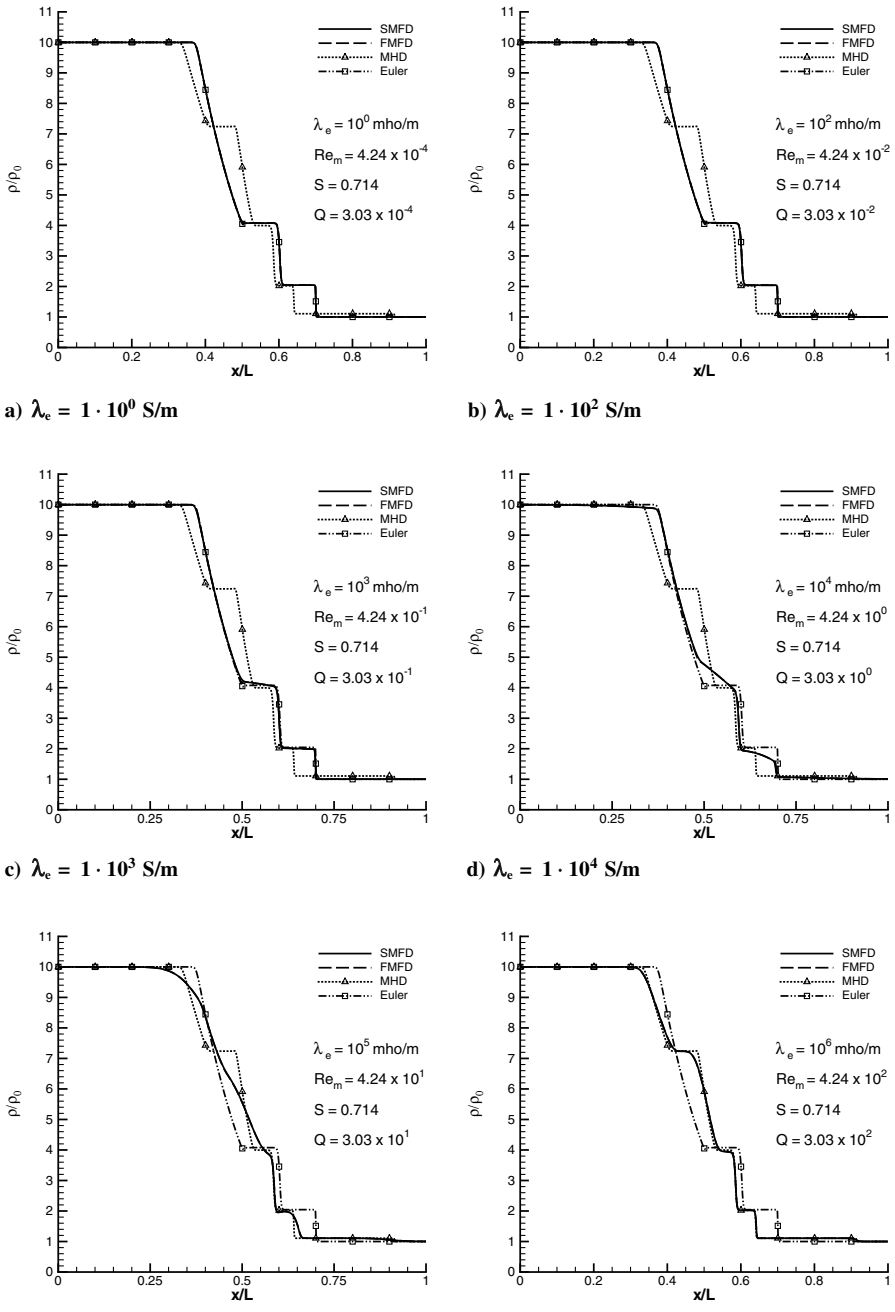

a) $\lambda_e = 1 \cdot 10^0$ S/m **b) $\lambda_e = 1 \cdot 10^2$ S/m**

c) $\lambda_e = 1 \cdot 10^3$ S/m **d) $\lambda_e = 1 \cdot 10^4$ S/m**

e) $\lambda_e = 1 \cdot 10^5$ S/m **f) $\lambda_e = 1 \cdot 10^6$ S/m**

Fig. 3 Density plots obtained using different values of λ_e in the considered shock-tube problem.

inaccurate results for low magnetic Reynolds numbers. To eliminate such difficulties, the SMFD equations can be solved in a "loosely coupled" fashion, as described in Secs. V.B.1 and V.B.2 below.

1. Governing Equations

Here, instead of dealing with the SMFD equations written in the form of Eqs. (11), we prefer to keep separate fluid dynamics and electromagnetic terms appearing under the divergence operator. Therefore, the momentum balance equation [Eq. (11b)] and the energy balance equation [Eq. (11c)] are rewritten as

$$\frac{\partial \rho v}{\partial t} + \nabla \cdot [p\bar{\bar{I}} + \rho \boldsymbol{v}\boldsymbol{v}] + \nabla \cdot \left[\gamma M^2 S \frac{B^2}{2} - \gamma M^2 S \boldsymbol{B}\boldsymbol{B}\right] - \frac{\sqrt{\gamma}M}{Re}\nabla \cdot \boldsymbol{\tau} = 0 \tag{56}$$

and

$$\begin{aligned}\frac{\partial(\rho e_m)}{\partial t} + \nabla \cdot [(\rho e_m + p)\boldsymbol{v}] + \frac{\sqrt{\gamma}M}{Re}\nabla \cdot (\boldsymbol{J}_U - \bar{\bar{\tau}} \cdot \boldsymbol{v}) + \gamma M^2 S \nabla \cdot [B^2 \boldsymbol{v} - (\boldsymbol{v} \cdot \boldsymbol{B})\boldsymbol{B}] + \frac{\sqrt{\gamma}M}{Re_m}\gamma M^2 S \nabla \cdot \{[\lambda_e^{-1}(\nabla \times \boldsymbol{B})] \times \boldsymbol{B}\} \\ = -\gamma M^2 S \boldsymbol{B} \cdot \nabla \times (\boldsymbol{v} \times \boldsymbol{B}) + \frac{\sqrt{\gamma}M}{Re_m}\gamma M^2 S \boldsymbol{B} \cdot \nabla \times [\lambda_e^{-1}(\nabla \times \boldsymbol{B})]\end{aligned} \tag{57}$$

Note that Eqs. (56) and (57) are perfectly equivalent to Eqs. (11b) and (11c), respectively.

In one dimension, the new form of the SMFD equations that is suitable to be integrated in a loosely coupled fashion is given by

$$\int_{x_1}^{x_2} \frac{\partial \boldsymbol{W}^{\mathbf{lcs}}}{\partial t}\,\mathrm{d}x + \boldsymbol{F}_2^{lcs,f} - \boldsymbol{F}_1^{lcs,f} + \boldsymbol{F}_2^{lcs,m} - \boldsymbol{F}_1^{lcs,m} = \int_{x_1}^{x_2} \boldsymbol{\Omega}^{\mathbf{lcs}}\,\mathrm{d}x \tag{58}$$

where

$$\boldsymbol{W}^{\mathbf{lcs}} = \begin{vmatrix} \rho \\ \rho u \\ \rho v \\ \rho w \\ \rho e_m \\ B_y \\ B_z \end{vmatrix}; \qquad \boldsymbol{F}^{\mathbf{lcs},f} = \begin{vmatrix} \rho u \\ \rho u u + p \\ \rho v u \\ \rho w u \\ (\rho e_m + p)u \\ 0 \\ 0 \end{vmatrix}; \qquad \boldsymbol{F}^{\mathbf{lcs},m} = \begin{vmatrix} 0 \\ C_1\left(\frac{B^2}{2} - B_x^2\right) \\ -C_1 B_y B_x \\ -C_1 B_z B_x \\ 0 \\ B_y u - v B_x \\ B_z u - w B_x \end{vmatrix} \tag{59}$$

and

$$\boldsymbol{\Omega}^{\mathbf{lcs}} = \begin{vmatrix} 0 \\ 0 \\ 0 \\ 0 \\ C_1\left\{C_2\left[\left(\frac{\partial B_y}{\partial x}\right)^2 + \left(\frac{\partial B_z}{\partial x}\right)^2\right] - \left[u\left(B_y\frac{\partial B_y}{\partial x} + B_z\frac{\partial B_z}{\partial x}\right) - B_x\left(v\frac{\partial B_y}{\partial x} + w\frac{\partial B_z}{\partial x}\right)\right]\right\} \\ C_2\left(\frac{\partial^2 B_y}{\partial x^2}\right) \\ C_2\left(\frac{\partial^2 B_z}{\partial x^2}\right) \end{vmatrix} \tag{60}$$

with

$$C_1 = \gamma M^2 S \tag{61a}$$

$$C_2 = \frac{\sqrt{\gamma}M}{Re_m}\frac{1}{\lambda_e} \tag{61b}$$

2. Numerical Method

The solution strategy that we choose to integrate Eqs. (58) in a loosely coupled fashion consists in using a flux-difference splitting Riemann solver [25] *conceived for fluid dynamics, and not for MHD* for evaluating the "fluid dynamics fluxes" $\boldsymbol{F}^{\mathbf{lcs},f}$, whereas the "magnetic fluxes" $\boldsymbol{F}^{\mathbf{lcs},m}$ are computed using a centered scheme. The source term $\boldsymbol{\Omega}^{\mathbf{lcs}}$ and the magnetic fluxes $\boldsymbol{F}^{\mathbf{lcs},m}$ are treated implicitly (except for the velocity components appearing in the magnetic induction equations), whereas the computation of fluid dynamics fluxes is explicit. The solution algorithm is

$$\frac{\tilde{\Delta}\boldsymbol{W}^{\mathbf{lcs}}}{\tilde{\Delta}t} + (\boldsymbol{F}^{lcs,f}_{N+1/2})^K - (\boldsymbol{F}^{lcs,f}_{N-1/2})^K + (\boldsymbol{F}^{lcs,m}_{N+1/2})^{K+1/2} - (\boldsymbol{F}^{lcs,m}_{N-1/2})^{K+1/2} = (\boldsymbol{\Omega}^{lcs}_N)^{K+\frac{1}{2}} \tag{62}$$

The solution procedure is composed of three steps:

Step 1: Solve the fluid dynamics Riemann problem to evaluate fluxes $\boldsymbol{F}^{\mathbf{lcs},fK}$ and also velocity components u and v at cells interfaces.

Step 2: Solve the magnetic induction equations (last two elements of Eq. (58)) implicitly, obtaining $\tilde{\Delta}B_y$ and $\tilde{\Delta}B_z$. As in the previous section, this requires the inversion of a tridiagonal matrix whose rank corresponds to the number of computational points in the domain:

$$[\boldsymbol{T}]\{\tilde{\Delta}B_i\} = -\{F^{B_i}\}^K \frac{\tilde{\Delta}t}{\Delta x} + \{\Omega^{B_i}\}^K \tilde{\Delta}t \tag{63}$$

The elements of the tridiagonal matrix $[\boldsymbol{T}]$ that is the subdiagonal term a, the diagonal term b, and the superdiagonal term c, are

$$a = -\left[\frac{\partial(F^{B_i})_{N-1/2}}{\partial(B_i)_{N-1}} + \frac{\partial(\Omega^{B_i})_N}{\partial(B_i)_{N-1}}\right]\frac{\tilde{\Delta}t}{2} = -\left[\frac{1}{2\Delta x}u_{N-1/2} + \frac{\sqrt{\gamma}M}{Re_m}\frac{1}{\lambda_e}\frac{l_3}{\Delta x^2}\right]\frac{\tilde{\Delta}t}{2} \tag{64a}$$

$$b = 1 + \left[\frac{\partial(F^{B_i})_{N+1/2}}{\partial(B_i)_N} - \frac{\partial(F^{B_i})_{N-1/2}}{\partial(B_i)_N} - \frac{\partial(\Omega^{B_i})_N}{\partial(B_i)_N}\right]\frac{\tilde{\Delta}t}{2} = 1 + \left[\frac{1}{2\Delta x}(u_{N+1/2} - u_{N-1/2}) - \frac{\sqrt{\gamma}M}{Re_m}\frac{1}{\lambda_e}\frac{l_3}{\Delta x^2}\right]\frac{\tilde{\Delta}t}{2} \tag{64b}$$

$$c = \left[\frac{\partial(F^{B_i})_{N+1/2}}{\partial(B_i)_{N+1}} - \frac{\partial(\Omega^{B_i})_N}{\partial(B_i)_{N+1}}\right]\frac{\tilde{\Delta}t}{2} = \left[\frac{1}{2\Delta x}u_{N+1/2} - \frac{\sqrt{\gamma}M}{Re_m}\frac{1}{\lambda_e}\frac{l_1}{\Delta x^2}\right]\frac{\tilde{\Delta}t}{2} \tag{64c}$$

Step 3: Solve mass, momentum, and energy balance equations, using fluxes $\boldsymbol{F}^{\mathbf{lcs},f}$ computed at step 1 and exploiting time-

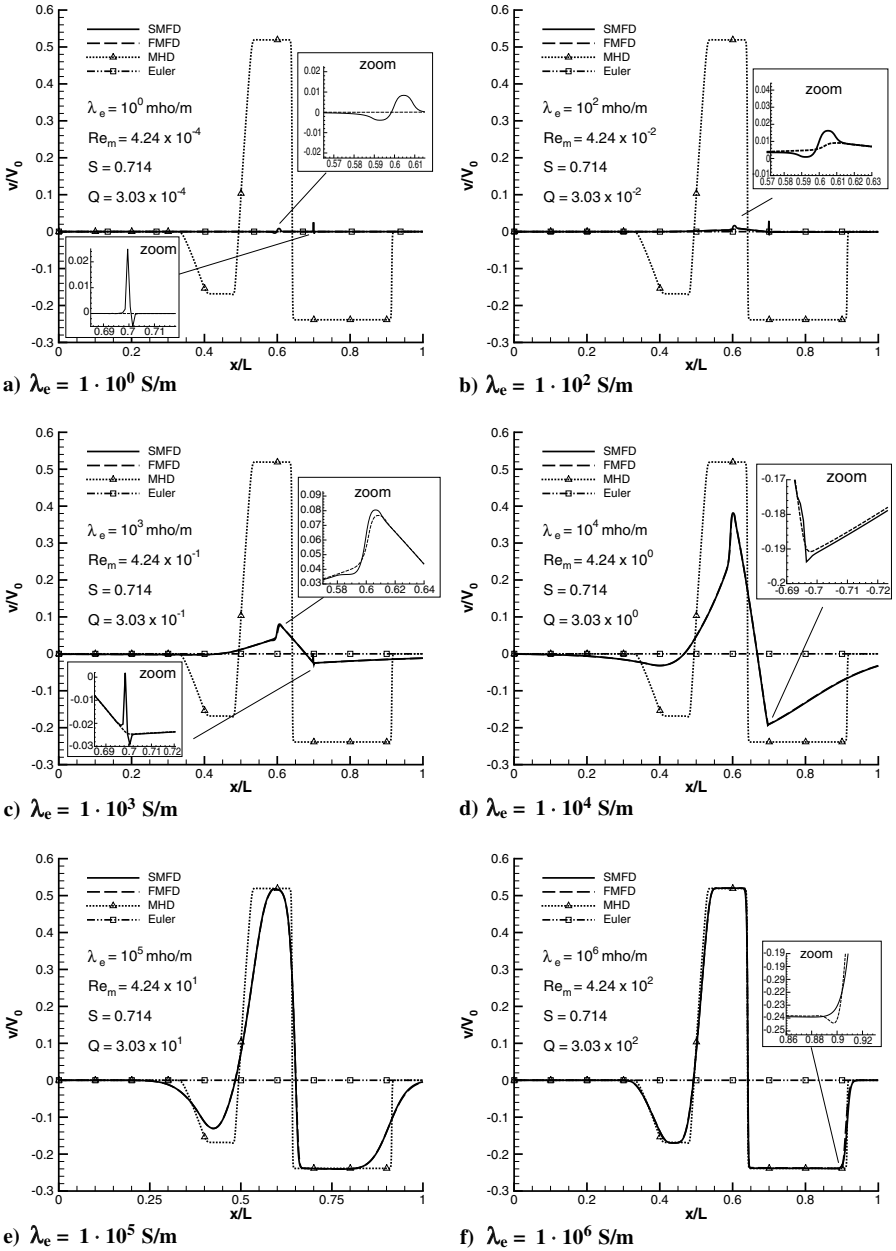

a) $\lambda_e = 1 \cdot 10^0$ S/m b) $\lambda_e = 1 \cdot 10^2$ S/m

c) $\lambda_e = 1 \cdot 10^3$ S/m d) $\lambda_e = 1 \cdot 10^4$ S/m

e) $\lambda_e = 1 \cdot 10^5$ S/m f) $\lambda_e = 1 \cdot 10^6$ S/m

Fig. 4 Velocity v plots obtained using different values of λ_e in the considered shock-tube problem.

increments $\tilde{\Delta}B_y$ and $\tilde{\Delta}B_z$ computed at step 2 for the implicit integration of $\boldsymbol{F}^{\mathbf{lcs},\boldsymbol{m}}$, and $\boldsymbol{\Omega}^{lcs}$. In particular, the solution algorithm for the momentum and the energy balance equations is

$$
\begin{aligned}
[\tilde{\Delta}(\rho u_i)] = &-\frac{\tilde{\Delta}t}{\Delta V}\{(F^{lcs,f})^{\rho u_i}_{N+1/2} - (F^{lcs,f})^{\rho u_i}_{N-1/2} \\
&+ C_1[(F^{lcs,m})^{\rho u_i}_{N+1/2} - (F^{lcs,m})^{\rho u_i}_{N-1/2}]\} \\
&- \frac{\tilde{\Delta}t}{\Delta V} C_1 \left\{ \left[\frac{\partial (F^{lcs,m})^{\rho u_i}}{\partial B_j} \right]_{N+1} \frac{(\tilde{\Delta}B_j)_{N+1}}{2} \right. \\
&\left. - \left[\frac{\partial (F^{lcs,m})^{\rho u_i}}{\partial B_j} \right]_{N-1} \frac{(\tilde{\Delta}B_j)_{N-1}}{2} \right\} \qquad (65)
\end{aligned}
$$

$$
\begin{aligned}
[\tilde{\Delta}(\rho e_m)] = &-\frac{\tilde{\Delta}t}{\Delta V}[(F^{lcs,f})^{\rho e_m}_{N+1/2} - (F^{lcs,f})^{\rho e_m}_{N-1/2}] \\
&+ (\Omega^{lcs})^{\rho e_m}\tilde{\Delta}t + \left\{ \frac{\partial (\Omega^{lcs})^{\rho e_m}_N}{\partial (B_j)_{N-1}} \frac{(\tilde{\Delta}B_i)_{N-1}}{2} \right. \\
&+ \frac{\partial (\Omega^{lcs})^{\rho e_m}_N}{\partial (B_j)_N} \frac{(\tilde{\Delta}B_i)_N}{2} + \frac{\partial (\Omega^{lcs})^{\rho e_m}_N}{\partial (B_j)_{N+1}} \frac{(\tilde{\Delta}B_i)_{N+1}}{2} \\
&\left. + \frac{\partial (\Omega^{lcs})^{\rho e_m}_N}{\partial (\rho u_i)_N} \frac{(\tilde{\Delta}\rho u_i)_N}{2} + \frac{\partial (\Omega^{lcs})^{\rho e_m}_N}{\partial (\rho)_N} \frac{(\tilde{\Delta}\rho)_N}{2} \right\} \tilde{\Delta}t \qquad (66)
\end{aligned}
$$

As it will be demonstrated in Sec. VII, the loosely coupled approach to the numerical solution of the SMFD equations is more accurate than the fully coupled approach for small values of the magnetic Reynolds number.

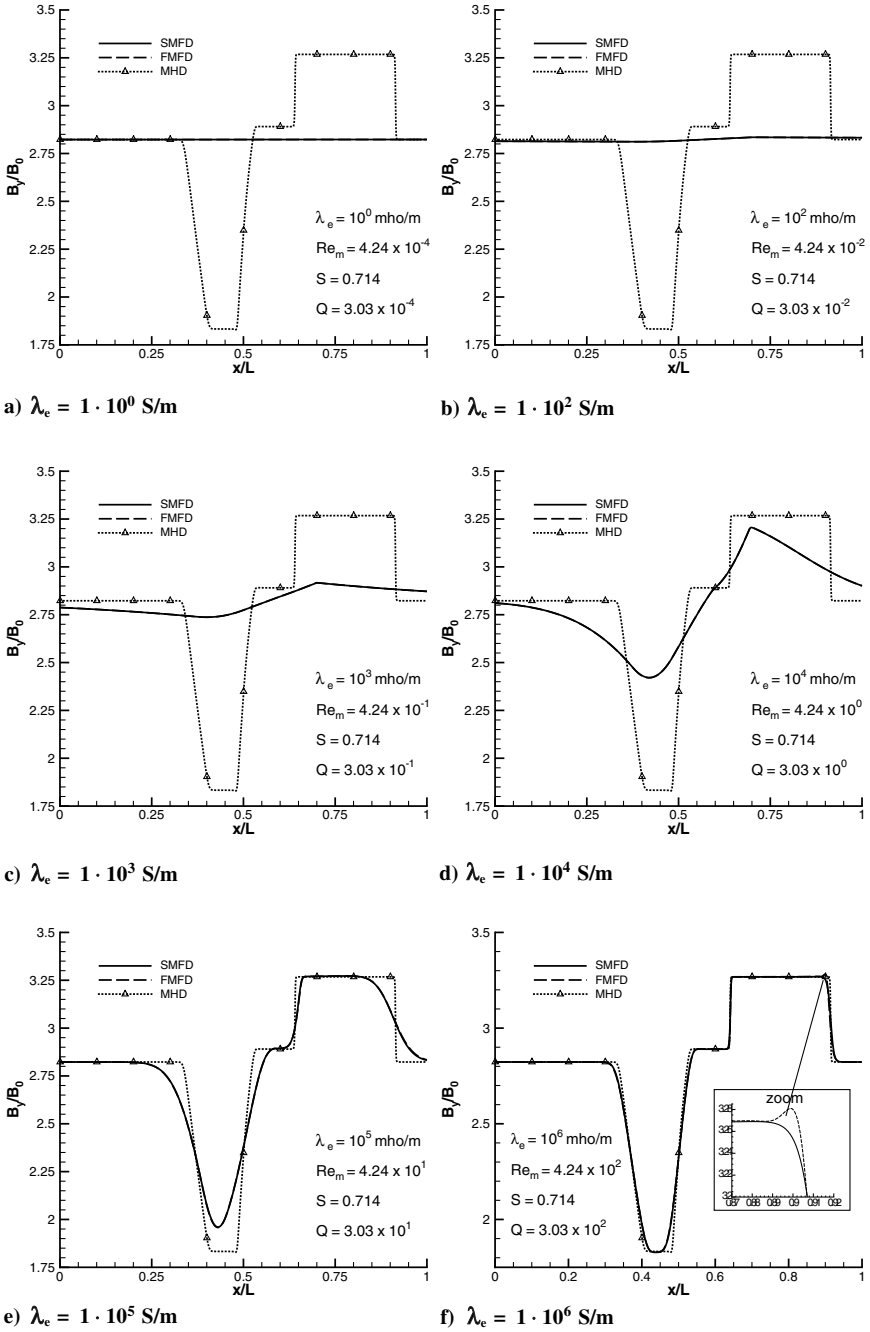

a) $\lambda_e = 1 \cdot 10^0$ S/m **b)** $\lambda_e = 1 \cdot 10^2$ S/m

c) $\lambda_e = 1 \cdot 10^3$ S/m **d)** $\lambda_e = 1 \cdot 10^4$ S/m

e) $\lambda_e = 1 \cdot 10^5$ S/m **f)** $\lambda_e = 1 \cdot 10^6$ S/m

Fig. 5 Magnetic field B_y plots obtained using different values of λ_e in the considered shock-tube problem.

VI. Numerical Solution of the Low Re_m Simplified Magnetofluid Dynamics Equations

A. Governing Equations

The low-Re_m SMFD model is described by Eqs. (15) and (16). In integral form, Eq. (15) reads like

$$\int_S (\lambda_e \nabla\phi)\cdot \boldsymbol{n}\, \mathrm{d}S - \int_S [\lambda_e(\boldsymbol{v}\times\boldsymbol{B})]\cdot \boldsymbol{n}\, \mathrm{d}S = 0 \tag{67}$$

and in general it can be solved as a pseudo-time-dependent equation adding an artificial time derivative of ϕ. In one dimension and under the assumption of constant and scalar electrical conductivity, Eq. (67) becomes

$$\left(\frac{\partial\phi}{\partial x}\right)_2 - \left(\frac{\partial\phi}{\partial x}\right)_1 = (vB_z - wB_y)_2 - (vB_z - wB_y)_1 \tag{68}$$

All the electric field components are constant, E_y and E_z because of the 1-D approximation, because $\frac{\partial\phi}{\partial y} = \frac{\partial\phi}{\partial z} = 0$, and E_x because of the assumption that $\rho_c = 0$, which implies that $\frac{\partial E_x}{\partial x} = 0$.

Thus, in the framework of our simplifying assumptions, the one-dimensional low-Re_m problem is reduced to the solution of the Euler equations as they appear in Eqs. (20a–20c), with constant $\boldsymbol{B}$ and $\boldsymbol{E}$.

B. Numerical Method

The Euler equations with electromagnetic source term are solved exactly as in the "fluid dynamics step" described in Sec. IV.B.

VII. Numerical Results

A. Shock-Tube Problem

The shock-tube problem can be seen as a particular Riemann problem with stationary initial conditions. In a Riemann problem, the collapse of the initial discontinuity generates a pattern of waves depending on the given initial left and right states. In fluid dynamics, three waves are generated: a contact discontinuity and two acoustic waves, that can be shocks or expansion fans (in general, there can be one expansion fan and one shock, or two shocks, or two expansion fans). In ideal magnetofluid dynamics (or magnetohydrodynamics, MHD), the presence of seven characteristic waves (one contact

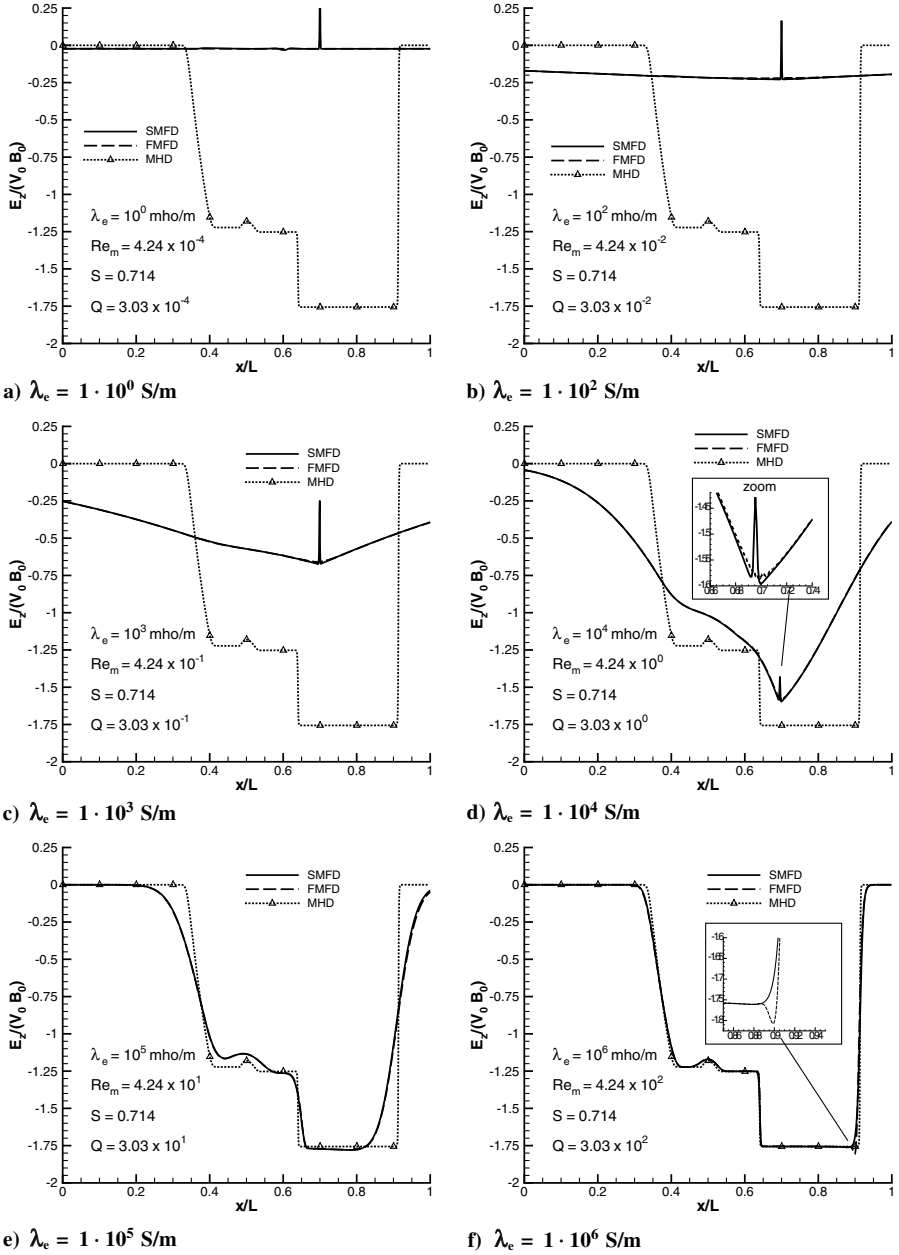

a) $\lambda_e = 1\cdot 10^0$ S/m b) $\lambda_e = 1\cdot 10^2$ S/m

c) $\lambda_e = 1\cdot 10^3$ S/m d) $\lambda_e = 1\cdot 10^4$ S/m

e) $\lambda_e = 1\cdot 10^5$ S/m f) $\lambda_e = 1\cdot 10^6$ S/m

Fig. 6 Electric field E_z plots obtained using different values of λ_e in the considered shock-tube problem.

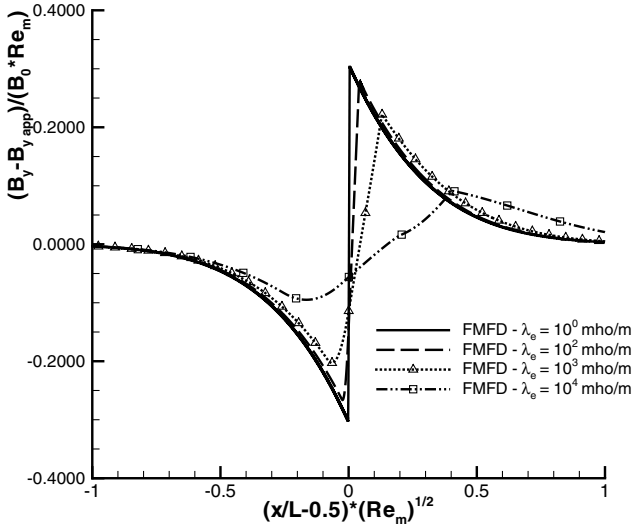

a) Re-scaled induced magnetic field, $\dfrac{B_y - B_{y_{app}}}{B_0 Re_m}$.

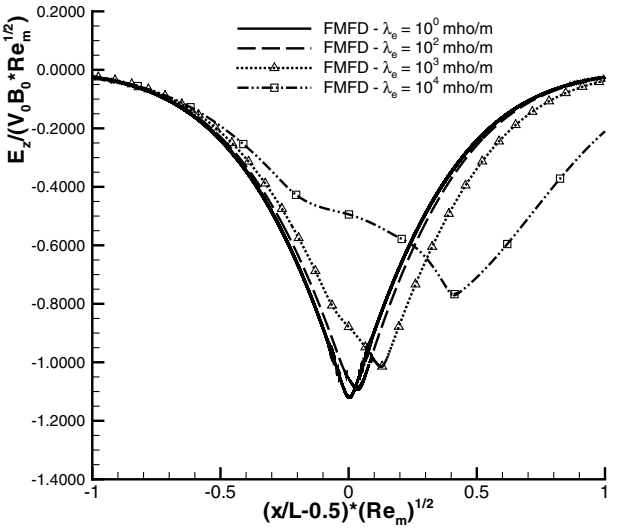

b) Re-scaled induced electric field, $\dfrac{E_z}{V_0 B_0 \sqrt{Re_m}}$.

Fig. 7 Induced magnetic and electric fields intensity for different values of λ_e.

discontinuity, two fast magnetoacoustic waves, two slow magnetoacoustic waves and two Alfvèn waves) allows for various possible configurations and the debate is still open about which are admissible and which are not [28,35–38].

If we restrict our scope to the particular case of the shock-tube problem, where the gas is initially stationary, then, in fluid dynamics, the two acoustic waves are certainly an expansion fan and a shock wave. In MHD, if we add the further conditions that the problem be planar, that is with magnetic field and velocity components lying on the same plane, and that the initial magnetic field be constant, we will certainly obtain a solution consisting of two magnetoacoustic expansion fans (a fast one and a slow one), two magnetoacoustic shock waves (a fast one and a slow one) and a contact discontinuity. Alfvèn waves are not present in planar problems.

B. Initial Conditions

We consider here a *planar* one-dimensional shock-tube problem, whose left- and right-side initial states are given in Table 1. With respect to the usual fluid dynamics test case, a uniform magnetic field is also applied, whereas the electric field is initially equal to zero. The gas is assumed to be electrically conductive, with uniform and scalar electrical conductivity. The results of various numerical experiments carried out with different values of λ_e, that is with different values of the magnetic Reynolds number Re_m, will be shown.

The similarity parameters that characterize the test case are given in Table 2. They were obtained using the reference values listed in Table 3. In particular, V_0 and B_0 have been chosen is such a way that $M = 1$ and $\gamma M^2 S = 1$.

We note that, in the *planar* one-dimensional shock-tube problem, the electric field component E_x cannot be generated. Thus, because

$$\nabla \cdot \boldsymbol{E} = \frac{\rho_c}{\varepsilon_0} \tag{69}$$

the electric-charge density must be null, unless a gradient of E_x is given as an initial condition. Here, we set the initial conditions such that $E_x = E_y = E_z = 0$ and, therefore, the fact of neglecting ρ_c in the full magnetofluid dynamics equations is an exact condition.

C. Boundary Conditions and Computational Domain

Left and right boundaries are placed sufficiently far from the initial discontinuity in such a way that they are not reached by any disturbance at the time when the solution is observed. Therefore, it is possible to enforce the undisturbed initial values of p, B_y, and E_z at the boundaries. Of course, to comply with the condition above, the computational domain has to be enlarged as the magnetic Reynolds number (or λ_e) decreases. The extension of the computational domain as a function of the electrical conductivity can be estimated in analogy with the first Stokes problem of fluid dynamics. The result is that we can assume that the magnetic "diffusive disturbance" penetrates in the domain as

$$\delta_{B_y} = 5.5\sqrt{\frac{\varepsilon_0 c^2}{\lambda_e} t} = 5.5L\sqrt{\frac{\bar{t}}{Re_m}} \gamma^{1/4} \sqrt{M} \tag{70}$$

where the coefficient equal to 5.5 is evaluated defining the penetration limit as the distance for which

$$\frac{(B_y)_{\text{ind}}}{(B_y)_{\text{app}}} \simeq 10^{-4} \tag{71}$$

The indication given by the gross estimate provided by Eq. (70) has been further refined by numerical simulations. The actual extension of the computational domains used in the numerical experiments, where computations were stopped at the nondimensional time $\bar{t} = 0.105$, is given in Table 4. In all cases, the initial discontinuity is placed at $x = 0.5$.

Table 5 Reinterpretation of the results shown in Figs. 2–6 considering a constant electrical conductivity $\lambda_e = 10^6$ but a variable reference length

L [m]	Re_m	t [s]	Figs. 2–6
10^0	4.24×10^2 ‘	3.675×10^{-4}	Figs. 2f, 3f, 4f, 5f, and 6f
10^{-1}	4.24×10^1	3.675×10^{-5}	Figs. 2e, 3e, 4e, 5e, and 6e
10^{-2}	4.24×10^0	3.675×10^{-6}	Figs. 2d, 3d, 4d, 5d, and 6d
10^{-3}	4.24×10^{-1}	3.675×10^{-7}	Figs. 2c, 3c, 4c, 5c, and 6c
10^{-4}	4.24×10^{-2}	3.675×10^{-8}	Figs. 2b, 3b, 4b, 5b, and 6b
10^{-6}	4.24×10^{-4}	3.675×10^{-10}	Figs. 2a, 3a, 4a, 5a, and 6a

D. Results

1. Full- vs Simplified Magnetofluid Dynamics

We present first a comparison between numerical simulations of the shock-tube problem illustrated in Sec. VII.B that were obtained solving the full magnetofluid dynamics (FMFD) equations as described in Sec. IV and the simplified magnetofluid dynamics (SMFD) equations as discussed in Sec. V. In particular, the fully coupled numerical approach of Sec. V.A.2 is used here for integrating the SMFD equations.

The basic computational grid is characterized by a constant spacing $\Delta x/L = 10^{-3}$. As mentioned above, the electrical conductivity is assumed to be uniform in our numerical experiments, and different tests will be carried out changing the magnitude of λ_e across a wide range of values. In Figs. 2–6, we show the results that are pertinent to electrical conductivities λ_e equal to 1, 10^2, 10^3, 10^4, 10^5, 10^6 S/m. Each figure shows the behavior of a different magnetogasdynamic variable. The borderline cases of null electrical conductivity, that is Euler flow, and of infinite electrical conductivity, that is MHD, are represented in the plots as a dash-dotted line with a square symbol and as dotted line with a triangle symbol, respectively. The intermediate cases of finite λ_e are plotted as a solid line when the solution was obtained solving the SMFD equations and as a dashed line when the FMFD equations were adopted.

As already anticipated, the pure fluid dynamic solution is characterized by a shock wave and a contact surface that move rightward and by an expansion fan whose outermost characteristics go leftward. The MHD solution contains a fast shock that moves rightward, followed by a slow shock and by a contact surface; a fast expansion fan moves leftward, whereas a slow-sonic slow expansion opens in both directions. Where the slow-sonic transition of the latter occurs, there is a change in sign of the velocity component v.

For small values of the electrical conductivity, the flowfield is very close to the Euler solution. The induced magnetic field is very small and it initially scales linearly with the magnetic Reynolds number, as shown in Fig. 7a, where B_y is rescaled as $(B_y - B_{y_{app}})/B_0 Re_m$. There, the nondimensional distance from the initial discontinuity, $x/L - 0.5$, is rescaled with $\sqrt{Re_m}$ to put in evidence the dependence from $\sqrt{Re_m}$ (for sufficiently small values of Re_m) of the magnetic field "diffusion," as described by Eq. (70). As Re_m gets larger, however, magnetic diffusion loses importance, the three waves structure is noticeably altered, and it finally takes the shape of the MHD solution for large values of λ_e. The magnitude of the induced magnetic field becomes important. The induced electric field behaves similarly to the induced magnetic field. The kink that is clearly visible on a level with the shock location for the SMFD solution is a numerical defect, as it will be explained later.

The FMFD and the SMFD solutions shown in Figs. 2–6 are almost perfectly one on top of the other. It should be noted that the source terms for the two models behave in a diametrically opposed way. In fact, in FMFD, small values of the magnetic Reynolds number mean small source terms, whereas the opposite it true in SMFD. Thus, having a small Re_m is an easy situation for solving the FMFD equations, but it is a *stiff* problem for SMFD. Conversely, a large Re_m does not create difficulties for computing the SMFD model, but it makes the solutions of the FMFD equations a difficult task.

In our tests, we experienced that the implicit treatment of source terms is largely beneficial to our computational methods. In fact, in the conditions of the present test case, we are able to satisfactorily run our codes up to $\lambda_e = 1 \times 10^6$ S/m using the FMFD model and, on the other hand, down to $\lambda_e = 1 \times 10^{-2}$ S/m with the SMFD model. These results are particularly stunning, as the wave structure of the homogenous part of the equations, which provides for a "fluid dynamic" three waves structure in FMFD and for a five waves structure in SMFD, is completely disrupted by the effect of the source terms, which produce five waves or three waves structures, respectively. In particular, the sharp numerical capture of "purely" *fluid dynamic* shocks with the SMFD code used at very low values of λ_e was unexpected.

Numerical difficulties are encountered by the FMFD solver only for $\lambda_e = 1 \times 10^6$ S/m and by the fast magnetoacoustic shock wave. A grid refinement analysis not shown here demonstrated that such a problem disappears increasing the number of grid points by a factor 10 (from 1000 points to 10,000 points). However, one should keep in

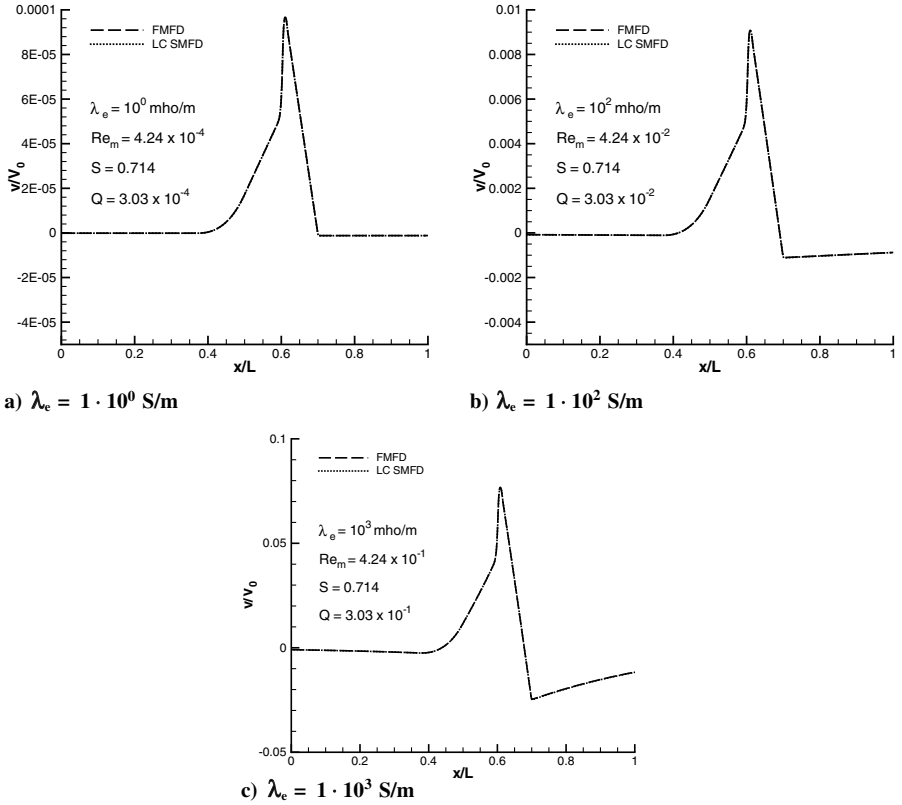

Fig. 8 Loosely coupled (LC) SMFD model vs FMFD model: comparison between velocity v plots.

mind that these values of λ_e represent the borderline for the numerical application of the FMFD solver.

On the other hand, the SMFD solver has a small problem, for values of λ_e smaller than 10^4 S/m, right at the locations of the fluid dynamic shock wave and of the contact surface. There, one can clearly see that the plots of the velocity component v display two kinks (Fig. 4), which are not present in the numerical solutions of the FMFD equations. A grid convergence analysis showed that, when the grid is refined, both disturbances remain, though their spatial extension is reduced due to the smaller grid spacing. In addition, the disturbance located at the contact surface position weakens as the grid is refined, whereas the one at the shock wave location does not change its magnitude significantly. The difficulties encountered by the SMFD solver for small values of Re_m can be physically justified noting that the results displayed in Figs. 2–6 for different values of λ_e can be interpreted in different ways depending whether the magnetic Reynolds number variation is imputed to a change of the electrical conductivity or to a change of the reference length. In the first case, Figs. 2–6, parts a)–f), which all refer to a nondimensional time $\bar{t} = 0.105$, must be interpreted as pictures of shock-tube problems with different electrical conductivities taken all at the same instant and focusing on the same spatial window. In the second case, they have to be considered as pictures of the same shock-tube problem (with a given electrical conductivity) taken at different instants and focusing on spatial windows whose extension is proportional to the physical time when the picture is shot. For instance, Figs. 2d, 3d, 4d, 5d, and 6d, which are characterized by $Re_m = 4.24 \times 10^0$, can be seen as pictures taken at $t = 3.675 \times 10^{-4}$ s showing a shock-tube problem with $\lambda_e = 10^4$ in the range (0 m $\leq x \leq$ 1 m), but also as pictures taken at $t = 3.675 \times 10^{-6}$ s showing a shock-tube problem with $\lambda_e = 10^6$ in the range (0 m $\leq x \leq$ 0.01 m). This second point of view is summarized in Table 5.

The discussion above implies that *any* shock-tube problem in magnetofluid dynamics (at least in the idealized form we are considering here, with uniform given λ_e) starts as a very low Re_m problem (in the limit for $t \to 0$ as a pure Euler flow) and then evolves toward an MHD problem. When integrating the SMFD equations, the use of an ideal MHD solver for evaluating "convective" fluxes is

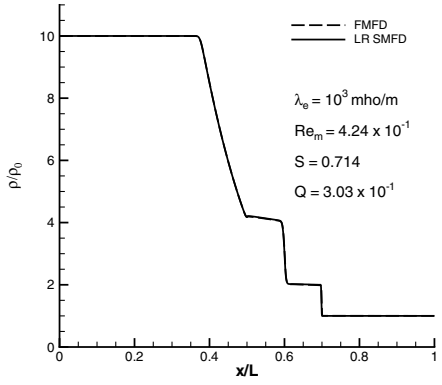

a) Density, $\lambda_e = 1 \cdot 10^3$ S/m

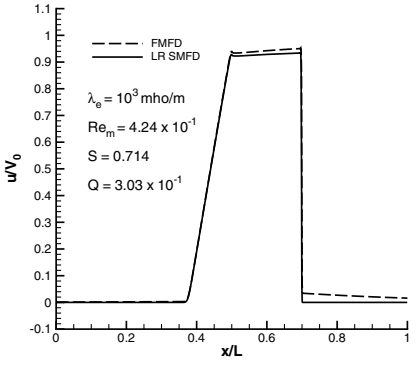

b) Velocity v, $\lambda_e = 1 \cdot 10^3$ S/m

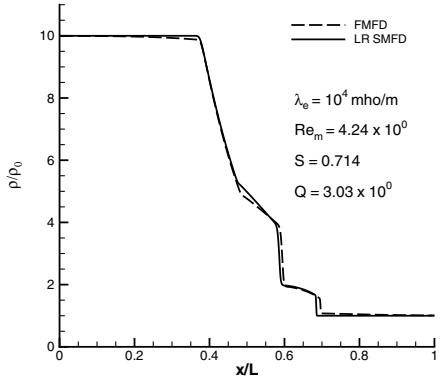

c) Density, $\lambda_e = 1 \cdot 10^4$ S/m

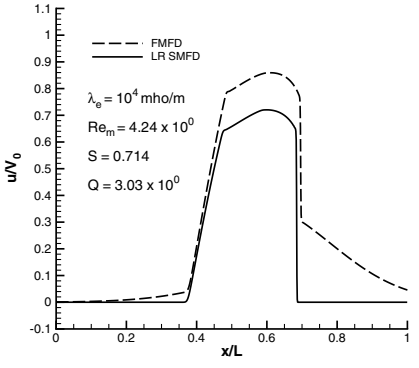

d) Velocity v, $\lambda_e = 1 \cdot 10^4$ S/m

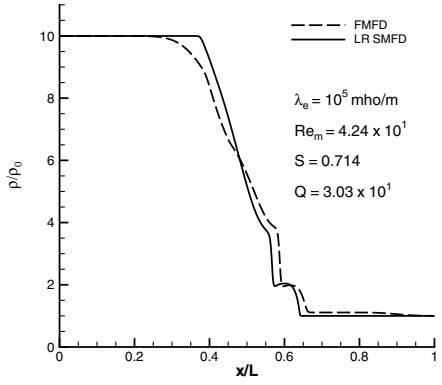

e) Density, $\lambda_e = 1 \cdot 10^5$ S/m

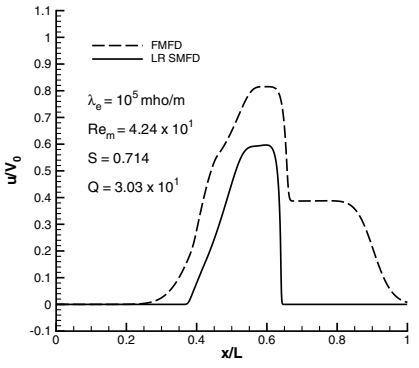

f) Velocity v, $\lambda_e = 1 \cdot 10^5$ S/m

Fig. 9 Low-Re_m approximation vs FMFD model: comparison between density and velocity v plots.

thus inadequate during the very first steps of integration, as diffusive terms are not able to balance and destroy the initial nonphysical jumps of v and B_y predicted by the ideal MHD solver. In particular, as "diffusive" fluxes are not present in the mass and momentum balance equations of the SMFD system, there is no mechanism to counterbalance the ideal MHD solution that is predicted at the first time-integration step for density and velocity components. Thus, after the first step of integration, the SMFD solutions for ρ, u, and v are those that would have been obtained in an ideal MHD computation, regardless of the Re_m of the considered problem. This is wrong, because a shock-tube problem in MFD begins as a fluid dynamics problem with $Re_m \to 0$. If we compare Riemann problem solutions for Euler and ideal MHD flows, we can see that the overall jumps of density are almost identical, that the overall jumps of u are not very different, but also that the jumps of v are completely different, as they are not present in the Euler solution. Such initial nonphysical jumps are responsible for the disturbances encountered at the contact surface location that we noticed in the SMFD solution in case of small Re_m, and they are particularly evident in the v velocity plots. As the numerical solution evolves in time, magnetic diffusion effects are *indirectly* transmitted to the mass and momentum balance equations through pressure and magnetic field. Grid refinement is beneficial, as demonstrated by a grid convergence study not included here, because, whereas the jumps in B_y and E_t predicted at the first time step by the ideal MHD solver are nondependent on the grid spacing, diffusive terms are and they are more efficient in flattening the B_y jump as Δx get smaller. As it will be shown in Sec. VII.D.2, disturbances can be completely eliminated using the loosely coupled SMFD approach, which is based on the solution of the SMFD equations using a fluid dynamics solver for convective fluxes rather than an ideal MHD solver.

As a final comment about SMFD and FMFD results, we note that the electric field component E_z (Fig. 6), which, within the SMFD model, is computed from the primitive variables using Eq. (45), presents a marked kink at the shock location. This happens because v is used to compute E_z and it is a consequence of the oscillation in v that exists there. A negligible disturbance is also present at the contact surface location for the same reason.

In conclusion, the numerical solutions obtained using the FMFD and SMFD models are both quite satisfactory. No differences can be perceived between the results related to the two approaches, except those mentioned above, where the FMFD model behaves better. Thus, the numerical solution of the FMFD equations in one dimension has been proved feasible and reliable, with a burden equal to a factor 3 in computing time.

2. *Loosely Coupled SMFD vs FMFD*

Results obtained using the loosely coupled SMFD approach described in Sec. V.B are shown in Fig. 8, where they are compared with results obtained solving the Full MFD equations (FMFD). In particular, the velocity component v is considered, as this is the variable where the inaccuracies in the SMFD solver were best evident. As it can be clearly seen, the two sets of results are practically identical and the kinks that were present in the SMFD solver results when the values of Re_m are small have completely disappeared. As anticipated above, this is due to the fact that the loosely coupled SMFD solver adopts a flux-difference splitting method conceived for fluid dynamics, rather than for MHD, for evaluating the fluxes in the mass, momentum and energy balance equations.

3. *Low-Re_m SMFD vs FMFD*

Results obtained using the low Re_m SMFD equations are presented in Fig. 9, where density and the velocity component u are plotted and compared with FMFD results. The intensity of the induced magnetic field cannot be neglected anymore (see also Fig. 5) for magnetic Reynolds numbers larger than 1, when the low Re_m approximation fails in predicting not only the magnitude of the fluid dynamics variables, but also the discontinuities propagation speed.

VIII. Conclusions

Four numerical methods, one for the *full magnetofluid dynamic equations* (FMFD), another for the *simplified magnetofluid dynamic equations* (SMFD), a third one for a loosely coupled approach to the SMFD equations and a fourth one for the low magnetic Reynolds number approximation have been developed and they are applied here to a shock-tube problem.

Results obtained using the FMFD and the SMFD model are compared first. In the considered test case, the two models are expected to provide exactly the same results, as it happens, in fact, in our numerical experiments. While the physical model based upon the SMFD equations is widely used in the scientific community, the FMFD model is rarely adopted. Here, we have shown that its numerical solution is feasible without an excessive burden in terms of computing time. The advantage of the FMFD model is that it could be used also in regions of the flow where terms containing the electric-charge density, which are neglected in the SMFD model, become important. In addition, the FMFD model is not indissolubly linked to the generalized Ohm law, in the sense that it allows for using any other constitutive law that relates the electric current with the other electromagnetic and fluid dynamic variables. Both numerical methods have proved to be very robust, as it was possible to use each of them in borderline situations in terms of magnitude of the magnetic Reynolds number. Nevertheless, some inaccuracies were detected in the SMFD results when the magnitude of the magnetic Reynolds number is small. We think that the latter can be attributed to the numerical procedure the SMFD approaches are usually based on, which consists in using a MHD solver to evaluate convective fluxes in the governing equations. Here we have demonstrated that such inaccuracies can be eliminated if a different approach, that we call the loosely coupled SMFD approach, is adopted.

Finally, results obtained using the low magnetic Reynolds number approximation are presented to investigate the limit of application of such an approach. In our numerical experiments, we found that the error contained in the numerical solution of the low-Re_m SMFD equations, when compared with the FMFD results, can be tolerated for values of Re_m smaller than about 1, but not above this value.

References

[1] Shang, J. S., Surzhikov, S. T., Kimmel, R., Gaitonde, D., Menart, J., and Hayes, J., "Mechanisms of Plasma Actuators for Hypersonic Flow Control," *Progress in Aerospace Sciences*, Vol. 41, 2005, pp. 642–668.

[2] Shang, J. S., "Recent Research in Magneto-Aerodynamics," *Progress in Aerospace Sciences*, Vol. 37, 2001, pp. 1–20.

[3] Giordano, D., "Hypersonic Flow Governing Equations with Electromagnetic Fields," AIAA Paper 2002-2165, May 2002.

[4] Shang, J. S., "Shared Knowledge in Computational Fluid Dynamics, Electromagnetics, and Magneto-Aerodynamics," *Progress in Aerospace Sciences*, Vol. 38, 2002, pp. 449–467.

[5] Sutton, G. W., and Sherman, A., *Engineering Magnetohydrodynamics*, McGraw–Hill, New York, 1965.

[6] Mitchner, M., and Kruger, C. H., *Partially Ionized Gases*, John Wiley & Sons, New York, 1973, Chap. 4.

[7] Prandtl, L., "Über die Flüssigkeitsbewegung bei sehr Kleiner Reibung," *Proceedings of the 3rd International Congress of Mathematics*, Heidelberg, Germany, 1904; English translation available as NACA TM-452, March 1928.

[8] Gaitonde, D., "A High-Order Implicit Procedure for the 3-D Electric Field in Complex Magnetogasdynamic Simulations," *Computers and Fluids*, Vol. 33, 2004, pp. 345–374.

[9] Shercliff, J. A., *A Textbook of Magnetohydrodynamics*, Pergamon Press Ltd., Oxford, 1965.

[10] Shumlak, U., and Loverich, J., "Approximate Riemann Solver for the Two-Fluid Plasma Model," *Journal of Computational Physics*, Vol. 187, 2003, pp. 620–638.

[11] Hakim, A., Shumlak, U., Aberle, C., and Loverich, J., "Maxwell Equations Solver for Plasma Simulations Based on Mixed Potential Formulation," AIAA Paper 2003-3829, June 2003.

[12] Damevin, H.-M., and Hoffmann, K. A., "Numerical Simulations of Hypersonic Magnetogasdynamics Flows over Blunt Bodies," AIAA Paper 2002-0201, Jan. 2002.

[13] Gaitonde, D. V., and Poggie, J., "Elements of a Numerical Procedure for 3-D MGD Flow Control Analysis," AIAA Paper 2002-198, Jan. 2002.
[14] Brio, M., and Wu, C. C., "An Upwind Differencing Scheme for the Equations of Ideal Magnetohydrodynamics," *Journal of Computational Physics*, Vol. 75, 1988, pp. 400–422.
[15] Powell, K. G., Roe, P. L., Myong, R. S., Gombosi, T., and Zeeuw, D. L. D., "An Upwind Scheme for Magnetohydrodynamics," AIAA Paper 95-1704-CP, 1995.
[16] Myong, R. S., and Roe, P. L., "On Gudonov-Type Schemes for Magnetohydrodynamics," *Journal of Computational Physics*, Vol. 147, 1998, pp. 545–567.
[17] MacCormack, R. W., "An Upwind Conservation Form Method for the Ideal Magnetohydrodynamics Equations," AIAA Paper 99-3609, June 1999.
[18] Linde, T. J., "A Three-Dimensional Adaptive Multifluid MHD Model for the Heliosphere," Ph.D. Thesis, Univ. of Michigan, 1998.
[19] Janhunen, P., "A Positive Conservative Method for Magnetohydrodynamics Based on HLL and Roe Methods," *Journal of Computational Physics*, Vol. 160, 2000, pp. 649–661.
[20] Xu, K., "Gas-Kinetic Theory Based Flux Splitting Method for Ideal Magnetohydrodynamics," ICASE Report 98-53, Nov. 1998.
[21] Dai, W., and Woodward, P. R., "A High-Order Godunov-Type Scheme for Shock Interactions in Ideal Magnetohydrodynamics," *SIAM Journal on Scientific Computing*, Vol. 18, No. 4, 1997, pp. 957–981.
[22] Sterk, H. D., Csíc, A., Abeele, D. V., Poedts, S., and Deconinck, H., "Stationary Two-Dimensional Magnetohydrodynamics Flows with Shocks: Characteristic Analysis and Grid Convergence Study," *Journal of Computational Physics*, Vol. 166, 2001, pp. 28–62.
[23] Augustinus, J., Hoffmann, K. A., and Harada, S., "Effect of Magnetic Field on the Structure of High-Speed Flows," *Journal of Spacecraft and Rockets*, Vol. 35, No. 5, 1998, pp. 639–646.
[24] Gaitonde, D. V., "High-Order Solution Procedure for Three-Dimensional Nonideal Magnetogasdynamics," *AIAA Journal*, Vol. 39, No. 11, 2001, pp. 2111–2120.
[25] Pandolfi, M., "A Contribution to the Numerical Prediction of Unsteady Flows," *AIAA Journal*, Vol. 22, No. 5, 1983, pp. 602–610.
[26] D'Ambrosio, D., "Numerical Prediction of Laminar Shock-Shock Interactions in Hypersonic Flow," *Journal of Spacecraft and Rockets*, Vol. 40, No. 2, 2003, pp. 153–161.
[27] Harten, A., Engquist, B., Osher, S., and Chakravarthy, S. R., "Uniformly High Order Accurate Essentially Non-Oscillatory Schemes, III," *Journal of Computational Physics*, Vol. 71, 1987, pp. 231–303.
[28] D'Ambrosio, D., and Pandolfi, M., "An Upwind Numerical Method for the Prediction of Ideal MHD High Speed Flows," AIAA Paper 2004-2164, June 2004.
[29] Powell, K. G., Roe, P. L., Linde, T. J., Gombosi, T. I., and Zeeuw, D. L. D., "A Solution-Adaptive Upwind Scheme for Ideal Magnetohydrodynamics," *Journal of Computational Physics*, Vol. 154, 1999, pp. 284–309.
[30] Tóth, G., "The $\nabla \cdot \boldsymbol{B} = 0$ Constraint in Shock-Capturing Magnetohydrodynamics Codes," *Journal of Computational Physics*, Vol. 161, 2000, pp. 605–652.
[31] Dedner, A., Kemm, F., Kröner, D., Munz, C.-D., Schnitzer, T., and Wesenberg, M., "Hyperbolic Divergence Cleaning for the MHD Equations," *Journal of Computational Physics*, Vol. 175, 2002, pp. 645–673.
[32] Tóth, G., and Roe, P. L., "Divergence- and Curl-Preserving Prolongation and Restriction Formulas," *Journal of Computational Physics*, Vol. 180, 2002, pp. 736–750.
[33] Londrillo, P., and Del Zanna, L. D., "On the Divergence-Free Condition in Godunov-Type Schemes for Ideal Magnetohydrodynamics: The Upwind Constrained Transport Method," *Journal of Computational Physics*, Vol. 195, 2004, pp. 17–48.
[34] Jeffrey, A., and Taniuti, T., *Non-Linear Wave Propagation: With Applications to Physics and Magnetohydrodynamics*, Academic Press, New York, 1964.
[35] Myong, R. S., and Roe, P. L., "Shock Waves and Rarefaction Waves in Magnetohydrodynamics. Part 2: The MHD System," *Journal of Plasma Physics*, Vol. 58, 1997, pp. 521–552.
[36] Myong, R. S., "Analytical Results on MHD Intermediate Shocks," *Geophysical Research Letters*, Vol. 24, No. 22, 1997, pp. 2929–2932.
[37] Torrilhon, M., "Non-Uniform Convergence of Finite Volume Schemes for Riemann Problems of Ideal Magnetohydrodynamics," *Journal of Computational Physics*, Vol. 192, 2003, pp. 73–94.
[38] Barmin, A. A., Kulikovskiy, A. G., and Pogorelov, N. V., "Shock-Capturing Approach and Nonevolutionary Solutions in Magnetohydrodynamics," *Journal of Computational Physics*, Vol. 126, 1996, pp. 77–90.